Perturbation theory for an Anderson quantum dot asymmetrically attached to two superconducting leads

M. Žonda,[1] V. Pokorný,[2,3] V. Janiš,[2] and T. Novotný[1]

[1]*Department of Condensed Matter Physics, Faculty of Mathematics and Physics, Charles University in Prague, Ke Karlovu 5, CZ-12116 Praha 2, Czech Republic*

[2]*Institute of Physics, The Czech Academy of Sciences, Na Slovance 2, CZ-18221 Praha 8, Czech Republic*

[3]*Theoretical Physics III, Center for Electronic Correlations and Magnetism, Institute of Physics, University of Augsburg, D-86135 Augsburg, Germany*

(Received 21 September 2015; published 29 January 2016)

Self-consistent perturbation expansion up to the second order in the interaction strength is used to study a single-level quantum dot with local Coulomb repulsion attached asymmetrically to two generally different superconducting leads. At zero temperature and a wide range of other parameters, the spin-symmetric version of the expansion yields excellent results for the position of the 0-π impurity quantum phase transition boundary and Josephson current together with the energy of Andreev bound states in the 0 phase as confirmed by numerical calculations using the numerical renormalization group method. We analytically prove that the method is charge conserving as well as thermodynamically consistent. Explicit formulas for the position of the 0-π phase boundary are presented for the Hartree-Fock approximation as well as for its variant called generalized atomic limit. It is shown that the generalized atomic limit can be used as a quick estimate for the position of the phase boundary at half-filling in a broad range of parameters. We apply our second-order perturbation method to the interpretation of the existing experimental data on the phase boundary with very satisfactory outcome, suggesting that the so-far employed heavy numerical tools such as numerical renormalization group and/or quantum Monte Carlo are not necessary in a class of generic situations and can be safely replaced by a perturbative approach.

DOI: 10.1103/PhysRevB.93.024523

I. INTRODUCTION

In the last decade, advances in the fabrication of nanodevices enabled to connect quantum dots with superconducting (SC) leads forming superconducting quantum dot nanostructures generalizing the conventional Josephson junctions [1]. Many experimental realizations of this concept using various BCS materials for the superconducting leads (Al, Pb, or Nb) and a great variety of quantum dots formed in semiconducting nanowires [2,3] or dots [4], carbon nanotubes [5–23], or even single C_{60} molecules [24] demonstrate the versatility of such setups. A major advantage of the superconducting quantum dots over conventional microscopic Josephson junctions lies in the possibility of a detailed control of their microscopic parameters, e.g., by tuning the onsite energy by a gate voltage. Such a high tunability is promising for potential applications of these hybrids in the nanoelectronics (e.g., as a superconducting single-electron transistor) or quantum computing as well as for detailed studies of their nontrivial physical properties.

These include Josephson supercurrent, Andreev subgap transport, and the way they are influenced by the zero-dimensional nature of the superconducting quantum dots with finite-size quantized levels and potentially strong effects of the local Coulomb interaction leading to strongly correlated phenomena such as the Kondo effect [25]. In many cases, the system can be very well described by a simplest single-impurity Anderson model (SIAM) coupled to BCS leads [26], which, depending on particular parameters, may exhibit so-called 0-π transition signaled by the sign reversal of the supercurrent [2,10,11,16,20,23]. The 0-π transition is induced by the underlying impurity quantum phase transition (QPT) related to the crossing of the lowest many-body eigenstates of the system from a spin-singlet ground state with positive supercurrent (0 phase) to a spin-doublet state with negative supercurrent (π phase) [26–36]. In single-particle spectral properties, this transition is associated with crossing of the Andreev bound states (ABS) at the Fermi energy as has also been observed experimentally [3,18,21].

A number of theoretical techniques have been used to address the 0-π transition and related properties of superconducting quantum dots. A very good quantitative agreement with the experiments [21,23,26] can be obtained in a wide range of parameters using heavy numerics such as numerical renormalization group (NRG) [21,30,32,37–42] and quantum Monte Carlo (QMC) [23,26,31,43]. However, both NRG and QMC are time and computational resources consuming. Alternative (semi)analytical methods based on various, often quite sophisticated, perturbation approaches either around noninteracting limit ($U = 0$) such as the mean-field theory [29,30,41,44], slave particles [33,45], and functional renormalization group (fRG) [35,46] or around the atomic limit ($\Gamma \to 0$ or $\Delta \to \infty$) [36,47,48] have been used for qualitative and in some limits even a quantitative description of the superconducting quantum dot properties. Yet, none of the mentioned methods with the exception of the mean-field/Hatree-Fock (HF) approximation are sufficiently simple and at the same time versatile to serve as a generic (semi)analytical solver. HF approximation has the attributes of the generic method [41], yet, it suffers from fundamental conceptual problems, namely, it identifies the 0-π transition with the point of breaking of the spin-symmetric solution and attributes the π phase to the magnetic solution of the self-consistent HF equations. This unphysical breaking of the spin symmetry together with the ensuing discontinuities of various physical quantities even at nonzero temperatures contradicting the experimental

observations disqualify the unrestricted HF approach as a reliable solver for the superconducting SIAM.

Surprisingly, with the exception of a few fragmented precursors [44,49], it has not been noticed until very recently [50,51] that the resummed perturbation theory incorporating second-order dynamical corrections to the spin-symmetric HF solution yields at zero temperature a nearly perfect description of the 0 phase for symmetric leads in a wide range of parameters. The aim of this work is to demonstrate that second-order perturbation theory is an efficient and reliable method not only for the symmetric leads, but also for a more general and realistic case of asymmetric tunnel coupling to different leads (i.e., with various values of superconducting gaps). This method is numerically much less expensive than NRG or QMC. Note that in the general case one has to deal with the two-channel Anderson model, therefore, the introduced second-order perturbation theory can be 10 or even 100 times faster (depending on parameters and used CPU cores) than the fully convergent NRG calculations. Simultaneously, this method gives nearly perfect results for the physical quantities in the 0 phase at zero temperature in a wide range of parameters corresponding to weakly and intermediately correlated regime, where the conventional deployment of NRG is unnecessary. As known from previous studies [30,37], the ground state in this regime is the BCS singlet in contrast to the strongly correlated regime where the ground state is the Kondo singlet. We illustrate this in Fig. 1 which depicts the ground-state phase diagram in the U-Δ plane for quantum dots with symmetric leads at half-filling. The crossover region between the BCS and Kondo singlets is approximately plotted as a gray stripe. The BCS singlet regime covers a broad range of parameters (note the logarithmic scale on the vertical axis) where second-order perturbation theory is in a nearly perfect agreement with NRG. Thus, we advocate this method to be the generic first-choice solver for the properties of the 0 phase.

In order to support this standpoint, we carefully examined formal properties of the approximation such as charge conservation, gauge invariance, and thermodynamic consistency

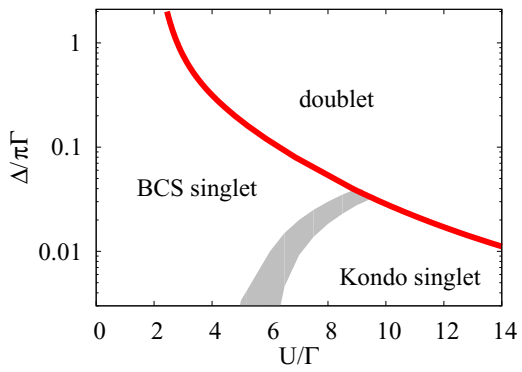

FIG. 1. Sketch of the phase diagram in the U-Δ plane of the superconducting single-impurity Anderson model with symmetric leads at half-filling. Full red line separates the singlet and doublet ground states and the shade region signals the crossover between the two kinds of singlet ground states. The perturbative approach presented in this paper works well in the whole BCS singlet regime as demonstrated in detail in Figs. 6 and 7.

and showed that it preserves all these important requirements.[1] Then, we systematically studied the zero-temperature 0-phase quantities in a wide parameter range, paying a special attention to the position of the phase boundary between the 0 and π phases. We identified the limits of applicability of our method by direct comparison with NRG data obtained via the NRG LJUBLJANA open source code [52,53]. At small enough temperatures, the boundary depends only weakly on temperature [35,43] and, therefore, our zero-temperature results are directly applicable to the existing experimental data. We finally compared our predictions with two experiments with excellent agreement, further justifying our claims.

The outline of the paper is as follows. In Sec. II, we introduce the superconducting SIAM, the Matsubara Green function methodology of the perturbation theory together with the Josephson current, and ABS formulas in the first subsection, while in the second part we study charge conservation, gauge invariance, and thermodynamic consistency conditions to be obeyed by approximations. In Sec. III, we introduce and analyze properties of the Hartree-Fock approximation and its dynamical corrections. In the following Sec. IV, after a brief summary of technical issues concerning the evaluation of the approximative equations, we present results for the position of the 0-π boundary first for the case of identical leads (equal SC gaps) and then for different leads with unequal gaps. Finally, in the last subsection we discuss in details the applicability and limitations of our method as demonstrated on various single-particle quantities in the 0 phase, such as ABS energies and/or induced SC gap. In Sec. V, we present comparison of quantitative results of our theory with two existing experiments on the position of the 0-π boundary. We conclude our work in the last Sec. VI. Supporting technical calculations for the HF boundary and charge conservation in the second-order perturbation theory are deferred to Appendixes A and B.

II. THEORY AND METHODS

A. Model and observables

We use a single-impurity Anderson model [21,26,31,32] as a model of the quantum dot with well-separated energy levels connected to two asymmetric superconducting leads [38]. The Hamiltonian of the system is given by

$$\mathcal{H} = \mathcal{H}_{\text{dot}} + \sum_{\alpha=R,L} \left(\mathcal{H}^{\alpha}_{\text{lead}} + \mathcal{H}^{\alpha}_{T}\right). \tag{1a}$$

The first term represents a single impurity with the level energy ε and the local Coulomb repulsion U:

$$\mathcal{H}_{\text{dot}} = \varepsilon \sum_{\sigma=\uparrow,\downarrow} d^{\dagger}_{\sigma} d_{\sigma} + U d^{\dagger}_{\uparrow} d_{\uparrow} d^{\dagger}_{\downarrow} d_{\downarrow}, \tag{1b}$$

where $d^{\dagger}_{\sigma}$ (d_{σ}) creates (annihilates) an electron with the spin σ on the impurity. The second term of Eq. (1a) is the BCS

[1]Its simplified version (DC) used for most of our numerical calculations strictly satisfies the charge conservation only for equal SC gaps and marginally breaks it for the general case (for details see Sec. IV C and Appendix B).

Hamiltonian of the leads

$$\mathcal{H}^{\alpha}_{\rm lead} = \sum_{\mathbf{k}\sigma} \epsilon_{\alpha}(\mathbf{k}) c^{\dagger}_{\alpha\mathbf{k}\sigma} c_{\alpha\mathbf{k}\sigma} - \Delta_{\alpha} \sum_{\mathbf{k}} (e^{i\Phi_{\alpha}} c^{\dagger}_{\alpha\mathbf{k}\uparrow} c^{\dagger}_{\alpha\ -\mathbf{k}\downarrow} + \text{H.c.}), \tag{1c}$$

with $\alpha = L, R$ denoting the left and right leads and $c^{\dagger}_{\alpha\mathbf{k}\sigma}$ ($c_{\alpha\mathbf{k}\sigma}$) creating (annihilating) conduction electrons. Finally, the hybridization term between the impurity and the contacts is given by

$$\mathcal{H}^{\alpha}_{T} = -t_{\alpha} \sum_{\mathbf{k}\sigma} (c^{\dagger}_{\alpha\mathbf{k}\sigma} d_{\sigma} + \text{H.c.}). \tag{1d}$$

All the studied quantities can be expressed with the help of the impurity one-electron (imaginary time/Matsubara) Green function (GF), which is a 2×2 matrix in the Nambu spinor formalism:

$$\begin{aligned} \widehat{G}_{\sigma}(\tau - \tau') &\equiv \begin{pmatrix} G_{\sigma}(\tau - \tau'), & \mathcal{G}_{-\sigma}(\tau - \tau') \\ \bar{\mathcal{G}}_{\sigma}(\tau - \tau'), & \bar{G}_{-\sigma}(\tau - \tau') \end{pmatrix} \\ &= -\begin{pmatrix} \langle \mathbb{T}[d_{\sigma}(\tau) d^{\dagger}_{\sigma}(\tau')] \rangle, & \langle \mathbb{T}[d_{\sigma}(\tau) d_{-\sigma}(\tau')] \rangle \\ \langle \mathbb{T}[d^{\dagger}_{-\sigma}(\tau) d^{\dagger}_{\sigma}(\tau')] \rangle, & \langle \mathbb{T}[d^{\dagger}_{-\sigma}(\tau) d_{-\sigma}(\tau')] \rangle \end{pmatrix} \\ &= \left(\right), \end{aligned} \tag{2}$$

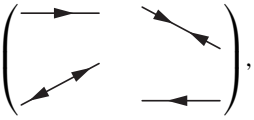

where the bar denotes the hole function. Since we only consider spin-symmetric solutions throughout the whole paper, we skip the spin index and we also set $e = \hbar = 1$ from now on. The exact form of the unperturbed ($U = 0$) impurity GF can be written as a function of Matsubara frequencies $\omega_n \equiv (2n+1)\pi/\beta$ (see Appendix A of Ref. [34]):

$$\widehat{G}_0(i\omega_n) = \begin{pmatrix} i\omega_n[1+s(i\omega_n)] - \varepsilon, & \Delta_{\Phi}(i\omega_n) \\ \Delta^{*}_{\Phi}(i\omega_n), & i\omega_n[1+s(i\omega_n)] + \varepsilon \end{pmatrix}^{-1}, \tag{3a}$$

where

$$s(i\omega_n) = \sum_{\alpha=L,R} \frac{\Gamma_{\alpha}}{\sqrt{\Delta^2_{\alpha} + \omega^2_n}} \tag{3b}$$

is the hybridization self-energy due to the coupling of the impurity to the superconducting leads. We have denoted by $\Gamma_{L,R} = \pi t^2_{L,R} \rho_{L,R}$ the normal-state tunnel-coupling magnitude (with $\rho_{L,R}$ being the normal-state density of states of the respective lead electrons at the Fermi energy) and

$$\Delta_{\Phi}(i\omega_n) = \sum_{\alpha=L,R} \frac{\Gamma_{\alpha}\Delta_{\alpha}}{\sqrt{\Delta^2_{\alpha} + \omega^2_n}} e^{i\Phi_{\alpha}}. \tag{3c}$$

The impact of the Coulomb repulsion $U > 0$ on the Green function is included in the interaction self-energy matrix $\widehat{\Sigma}(i\omega_n) \equiv \left(\begin{smallmatrix} \Sigma(i\omega_n), & \mathcal{S}(i\omega_n) \\ \bar{\mathcal{S}}(i\omega_n), & \bar{\Sigma}(i\omega_n) \end{smallmatrix}\right)$, so that the full propagator in the spin-symmetric situation is determined by the Dyson equation $\widehat{G}^{-1}(i\omega_n) = \widehat{G}^{-1}_0(i\omega_n) - \widehat{\Sigma}(i\omega_n)$. Symmetry relations for the spin-symmetric version of the Green function [Eq. (2)] reformulated in the Matsubara representation [46, Sec. 9.3.3] are $\bar{G}(i\omega_n) = -G^{*}(i\omega_n) = -G(-i\omega_n)$ and $\bar{\mathcal{G}}(i\omega_n) = \mathcal{G}^{*}(i\omega_n) = \mathcal{G}^{*}(-i\omega_n)$. The same applies to the self-energies, i.e., $\bar{\Sigma}(i\omega_n) = -\Sigma^{*}(i\omega_n) = -\Sigma(-i\omega_n)$, $\bar{\mathcal{S}}(i\omega_n) = \mathcal{S}^{*}(i\omega_n) = \mathcal{S}^{*}(-i\omega_n)$. Here, the asterisk stands for time inversion being complex conjugation in the Matsubara formalism. Consequently, the interacting Green function explicitly reads as

$$\widehat{G}(i\omega_n) = -\frac{1}{D(i\omega_n)} \begin{pmatrix} i\omega_n[1+s(i\omega_n)] + \varepsilon + \Sigma^{*}(i\omega_n), & -\Delta_{\Phi}(i\omega_n) + \mathcal{S}(i\omega_n) \\ -\Delta^{*}_{\Phi}(i\omega_n) + \mathcal{S}^{*}(i\omega_n), & i\omega_n[1+s(i\omega_n)] - \varepsilon - \Sigma(i\omega_n) \end{pmatrix}. \tag{4}$$

The existence and the position of the ABS are determined by zeros of the negative determinant of the inverse Green function (i.e., poles of the Green function)

$$\begin{aligned} D(i\omega_n) &\equiv -\det[\widehat{G}^{-1}(i\omega_n)] = \omega^2_n[1+s(i\omega_n)]^2 \\ &\quad + |\varepsilon + \Sigma(i\omega_n)|^2 + |\Delta_{\Phi}(i\omega_n) - \mathcal{S}(i\omega_n)|^2 \\ &= D(-i\omega_n) = D^{*}(i\omega_n) \geqslant 0. \end{aligned} \tag{5}$$

The determinant analytically continued from Matsubara to the real frequency axis is real within the gap and can go through zero $D(\omega_0) = 0$ determining the (real) in-gap energies $\pm\omega_0$ of the ABS symmetrically placed around the Fermi energy lying in the middle of the gap. ABS are crucial for transport of the Cooper pairs through the quantum dot because they usually provide the dominant contribution to the dissipationless Josephson current through the impurity. Furthermore, their crossing at the Fermi energy determines the phase boundary between 0 and π phases as their zero energy is equivalent to the degeneracy of the two lowest-energy many-body eigenstates of the system, which is the point of the impurity QPT [21].

The Josephson current out of the dot into the respective reservoir J_{α} is defined from the Heisenberg equation of motion for the particle number in the reservoir $J_{\alpha} \equiv d\langle \sum_{\mathbf{k}} c^{\dagger}_{\alpha\mathbf{k}\sigma} c_{\alpha\mathbf{k}\sigma} \rangle / dt = -i\langle [\sum_{\mathbf{k}} c^{\dagger}_{\alpha\mathbf{k}\sigma} c_{\alpha\mathbf{k}\sigma}, \mathcal{H}] \rangle$ and can be evaluated as a Matsubara sum of the anomalous Green function

$$\begin{aligned} J_{\alpha} &= \frac{2}{\beta} \text{Im} \sum_{\omega_n} \frac{\Gamma_{\alpha}}{\sqrt{\Delta^2_{\alpha} + \omega^2_n}} \\ &\quad \times \text{Tr}\left[\begin{pmatrix} 0 & -\Delta_{\alpha} e^{i\Phi_{\alpha}} \\ \Delta_{\alpha} e^{-i\Phi_{\alpha}} & 0 \end{pmatrix} \widehat{G}(i\omega_n) \right] \\ &= \frac{2}{\beta} \text{Im} \sum_{\omega_n} \frac{\Gamma_{\alpha}\Delta_{\alpha}}{\sqrt{\Delta^2_{\alpha} + \omega^2_n}} [\mathcal{G}(i\omega_n) e^{-i\Phi_{\alpha}} - \bar{\mathcal{G}}(i\omega_n) e^{i\Phi_{\alpha}}] \\ &= \frac{4}{\beta} \sum_{\omega_n} \frac{\Gamma_{\alpha}\Delta_{\alpha}}{\sqrt{\Delta^2_{\alpha} + \omega^2_n}} \text{Im}[\mathcal{G}(i\omega_n) e^{-i\Phi_{\alpha}}], \end{aligned} \tag{6}$$

where $\alpha = L, R$ as before. For any approximative treatment such as our perturbation expansion in U there always arises an important question of charge conservation, i.e., whether $J_L = -J_R$ and thermodynamic consistency, i.e., whether Josephson current calculated by different approaches, e.g., directly from

Eq. (6) or as a phase derivative of the associated free energy, gives the same. We devote the following subsection to these nontrivial fundamental questions.

B. Charge conservation, thermodynamic consistency, and gauge invariance

Any consistent approximation must respect charge conservation, i.e., the Josephson currents through the left and right interfaces sum up to zero (due to the above convention for the definition of the Josephson current as flowing *into* the respective lead). The condition $J_L + J_R = 0$ can be rewritten with the help of the second line of Eq. (6) as

$$\begin{aligned} 0 &= \frac{2}{\beta}\mathrm{Im}\sum_{\omega_n,\alpha}\frac{\Gamma_\alpha\Delta_\alpha}{\sqrt{\Delta_\alpha^2+\omega_n^2}}[\mathcal{G}(i\omega_n)e^{-i\Phi_\alpha} - \mathcal{G}^*(i\omega_n)e^{i\Phi_\alpha}] \\ &= \frac{2}{\beta}\mathrm{Im}\sum_{\omega_n}[\Delta_\Phi^*(i\omega_n)\mathcal{G}(i\omega_n) - \Delta_\Phi(i\omega_n)\mathcal{G}^*(i\omega_n)] \\ &= \frac{2}{\beta}\mathrm{Im}\sum_{\omega_n}[\mathcal{S}^*(i\omega_n)\mathcal{G}(i\omega_n) - \mathcal{S}(i\omega_n)\mathcal{G}^*(i\omega_n)] \\ &= \frac{4}{\beta}\mathrm{Im}\sum_{\omega_n}\mathcal{S}^*(i\omega_n)\mathcal{G}(i\omega_n)\,, \end{aligned} \tag{7}$$

where we used $\Delta_\Phi(i\omega_n) = D(i\omega_n)\mathcal{G}(i\omega_n) + \mathcal{S}(i\omega_n)$ from Eq. (4) and reality of $D(i\omega_n)$ from Eq. (5). For symmetric leads one can choose real $\Delta_\Phi(i\omega_n)$ and, consequently, the anomalous self-energy and Green function fulfill $\mathcal{S}^*(i\omega_n) = \mathcal{S}(-i\omega_n)$ and $\mathcal{G}^*(i\omega_n) = \mathcal{G}(-i\omega_n)$. The charge-conservation condition (7) is then satisfied automatically as can be seen by the change of the summation variable $\omega_n \to -\omega_n$. Since for asymmetric leads one cannot guarantee the reality of $\Delta_\Phi(i\omega_n)$ for all frequencies and thus $\mathcal{S}^*(i\omega_n) \neq \mathcal{S}(-i\omega_n)$ approximations must be checked for fulfilling charge conservation (7) by explicit verification.

Apart from a direct approach to charge conservation via the explicit formula for the Josephson current [Eq. (6)], we may also employ an indirect one starting with the phase-dependent grand potential ("free energy") of the system. The dissipationless Josephson current can also be determined as the phase derivative of the thermodynamic potential. Approximate calculations of a thermodynamic quantity (such as the Josephson current here) lead to the same result when different equivalent representations are used only in *thermodynamically consistent* approaches in the Baym sense [54,55].

A thermodynamically consistent approximation can be generated from a Luttinger-Ward functional $\phi[\widehat{G}]$. It is represented in terms of the full one-electron Green function $\widehat{G}$ [Eq. (4)], from which the self-energy is determined via a functional derivative. In our case, with asymmetric leads we have to treat both electron and hole variables as independent parameters. Hence, the functional derivates determining the self-energies read as $\Sigma(i\omega_n) = \beta\delta\phi[\widehat{G}]/\delta G^*(-i\omega_n)$ for the normal part and $\mathcal{S}(i\omega_n) = \beta\delta\phi[\widehat{G}]/\delta\mathcal{G}^*(-i\omega_n)$ for the anomalous one and analogously for the self-energies $\Sigma^*(i\omega_n)$ and $\mathcal{S}^*(i\omega_n)$. The grand potential then contains both electron and hole variables, where the hole variables are decorated with asterisks that have the meaning of complex conjugation (only) in equilibrium. The grand potential can be represented with the aid of the Luttinger-Ward functional as follows:

$$\begin{aligned} 2\Omega[\widehat{G},\widehat{\Sigma}] = \phi[\widehat{G}] - \frac{1}{\beta}\sum_{\omega_n} e^{i\omega_n 0^+}\{&G(i\omega_n)\Sigma^*(-i\omega_n) + G^*(-i\omega_n)\Sigma(i\omega_n) + \mathcal{G}(i\omega_n)\mathcal{S}^*(-i\omega_n) + \mathcal{G}^*(-i\omega_n)\mathcal{S}(i\omega_n) \\ &+ \ln[\{i\omega_n[1+s(i\omega_n)] - \varepsilon - \Sigma(i\omega_n)\}\{i\omega_n[1+s(i\omega_n)] + \varepsilon + \Sigma^*(i\omega_n)\} \\ &- [\Delta_\Phi(i\omega_n) - \mathcal{S}(i\omega_n)][\Delta_\Phi^*(i\omega_n) - \mathcal{S}^*(i\omega_n)]]\}. \end{aligned} \tag{8}$$

Complex variables $G(i\omega_n), G^*(i\omega_n)$, $\Sigma(i\omega_n), \Sigma^*(i\omega_n)$ as well as $\mathcal{G}(i\omega_n), \mathcal{G}^*(i\omega_n)$, $\mathcal{S}(i\omega_n), \mathcal{S}^*(i\omega_n)$ are variational parameters the physical values of which are determined from the stationarity of the grand potential $\Omega[\widehat{G},\widehat{\Sigma}]$. Due to the electron-hole symmetry, the electron and hole contributions to the thermodynamic potential are identical, hence, the factor 2 on the left-hand side. An approximation is thermodynamically consistent and conserving if we are able to determine explicitly the Luttinger-Ward functional $\phi[\widehat{G}]$. Such approximations are called ϕ derivable.

Reliable and physically acceptable approximations should not only be thermodynamically consistent but must be gauge invariant. Observables in Josephson junction setups depend on the phase difference between the leads but they cannot depend on the absolute values of the two phases. In other words, the physics must be invariant with respect to a global phase shift $\Phi_{L,R} \mapsto \Phi_{L,R} + \Delta\Phi$, which is a manifestation of gauge invariance. Obviously, the building elements of the theory, the Green functions (3a) and (4), are not invariant and we must always check that they enter the measurable quantities, such as the supercurrent (6), in a way that preserves gauge invariance. The resulting self-energy $\widehat{\Sigma}(i\omega_n)$ and consequently $\widehat{G}(i\omega_n)$ transform equally as $\widehat{G}_0(i\omega_n)$ [Eq. (3a)] under the gauge transformation in thermodynamically consistent approximations. That is, only the off-diagonal elements pick up the global phase shift (with the respective sign) from which we can immediately see that the Josephson current (6) is indeed gauge invariant as it should be.

We can also use the functional of the grand potential $\Omega[\widehat{G},\widehat{\Sigma}]$ to prove gauge invariance of a ϕ-derivable approximation. In gauge-invariant theories, thermodynamic potentials depend only on the phase difference, i.e., $\Omega[\widehat{G},\widehat{\Sigma}](\Phi_L,\Phi_R) \equiv \Omega[\widehat{G},\widehat{\Sigma}](\Phi_L - \Phi_R)$. Consequently, charge conservation $J_L \equiv \frac{\partial\Omega[\widehat{G},\widehat{\Sigma}](\Phi_L-\Phi_R)}{\partial\Phi_L} = -\frac{\partial\Omega[\widehat{G},\widehat{\Sigma}](\Phi_L-\Phi_R)}{\partial\Phi_R} \equiv -J_R$ immediately follows.

III. APPROXIMATION SCHEMES

Since the exact expression for the self-energy of the superconducting Anderson impurity model is unknown, we

have applied the standard Matsubara resummed perturbation theory in the interaction strength U to summing up one-particle-irreducible diagrams for the self-energy in terms of the dressed one-particle Green function. To avoid the unphysical spin polarization of the impurity, which can be easily obtained within the resummed (dressed) approach from the self-consistent solution of a nonlinear equation for the single-particle Green function, we restrict the solution to the spin-symmetric case. This results in the situation when for certain parameters at zero temperature there exists no solution for the Green function. The breakdown of the solution coincides with the crossing of ABS energies at the Fermi energy, i.e., with the 0-π quantum phase transition. Thus, while the 0 phase, which can be smoothly connected with the noninteracting case $U = 0$, can be captured by the perturbative approach, the π phase with doubly degenerate ground state is beyond the reach of this simple perturbation theory. We explicitly demonstrate this concept for the Hartree-Fock solution, where all quantities at QPT can be addressed analytically, but the same scheme carries over to higher orders of the perturbation theory, in particular to second order, being the main focus of our study. The very possibility of a description of the π phase within a (suitably modified) perturbative approach remains an open question as we discuss in more detail later in Sec. IV C.

A. Spin-symmetric (restricted) Hartree-Fock approximation

Mathematical expressions for first-order perturbation expansion in U, Hartree-Fock (HF) contributions, read as

$$\Sigma^{\mathrm{HF}} = \frac{U}{\beta}\sum_{\omega_n} G^{\mathrm{HF}}(i\omega_n)e^{i\omega_n 0^+} = \tag{9a}$$

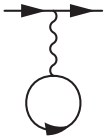

and

$$\mathcal{S}^{\mathrm{HF}} = \frac{U}{\beta}\sum_{\omega_n} \mathcal{G}^{\mathrm{HF}}(i\omega_n) = \tag{9b}$$

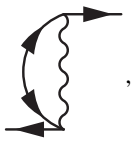

where the HF Green function reads as

$$\widehat{G}^{\mathrm{HF}}(i\omega_n) = -\frac{1}{D^{\mathrm{HF}}(i\omega_n)}\begin{pmatrix} i\omega_n[1+s(i\omega_n)]+\varepsilon+\Sigma^{\mathrm{HF}}, & -\Delta_\Phi(i\omega_n)+\mathcal{S}^{\mathrm{HF}} \\ -\Delta_\Phi^*(i\omega_n)+\mathcal{S}^{\mathrm{HF}*}, & i\omega_n[1+s(i\omega_n)]-\varepsilon-\Sigma^{\mathrm{HF}} \end{pmatrix}, \text{ with the determinant} \tag{9c}$$

$$D^{\mathrm{HF}}(i\omega_n) = \omega_n^2[1+s(i\omega_n)]^2 + |\varepsilon+\Sigma^{\mathrm{HF}}|^2 + |\Delta_\Phi(i\omega_n)-\mathcal{S}^{\mathrm{HF}}|^2. \tag{9d}$$

The hole (asterisks) functions are obtained from complex conjugation of the equations for the electron functions. Obviously, the frequency-independent self-energy of the HF approximation neglects any dynamical correlations caused by particle interaction. Nevertheless, it is still capable to describe qualitatively the 0-π quantum phase transition even without the necessity of the common, yet questionable [29,41,44], breaking of spin-reflection symmetry [50,51]. Therefore, it is a useful demonstration tool of the basic ideas concerning the model as well as a worthy etalon of more elaborate methods. The explicit formula for the HF phase boundary for the completely symmetric case $\Delta_L = \Delta_R$, $\Gamma_L = \Gamma_R$ was derived in our previous work [50]; here we provide a general solution.

Before that, though, we discuss charge-conservation and gauge-invariance properties of the HF approximation. If we insert Eq. (9b) into the last line of Eq. (7), we see that it is satisfied. Thus, the HF self-energy yields a charge-conserving approximation. Similarly, the HF self-energy transforms under the gauge transformation identically to the (dressed) Green function as it should. Furthermore, HF self-energy can be derived from a manifestly gauge-invariant Luttinger-Ward functional

$$\phi^{\mathrm{HF}}[\widehat{G}] = \frac{U}{\beta^2}\sum_{\omega_n,\omega_k}\{e^{i(\omega_n-\omega_k)0^+}G(i\omega_n)G^*(i\omega_k) + \mathcal{G}(i\omega_n)\mathcal{G}^*(i\omega_k)\}$$

$$= \quad + \tag{9e}$$

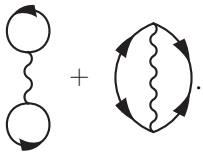

Consequently, HF approximation is both charge conserving as well as thermodynamically consistent.

Now, we turn to the calculation of the HF phase boundary. The self-consistent HF equations read as

$$\Sigma^{\mathrm{HF}} = -\frac{U}{\beta}\sum_{\omega_n} e^{i\omega_n 0^+}\frac{i\omega_n[1+s(i\omega_n)]+\Sigma^{\mathrm{HF}}+\varepsilon}{D^{\mathrm{HF}}(i\omega_n)},$$
$$\mathcal{S}^{\mathrm{HF}} = -\frac{U}{\beta}\sum_{\omega_n}\frac{\mathcal{S}^{\mathrm{HF}}-\Delta_\Phi(i\omega_n)}{D^{\mathrm{HF}}(i\omega_n)}. \tag{10}$$

Further manipulations of the above equations stated in Appendix A lead to the following set of equations at zero temperature (since we are interested in the phase boundary) for the auxiliary quantities $E_d \equiv \Sigma^{\mathrm{HF}} + \varepsilon$ and $\delta \equiv \sum_{\alpha=L,R} \Gamma_\alpha e^{i\Phi_\alpha} - \mathcal{S}^{\mathrm{HF}}$:

$$E_d = \varepsilon + \frac{U}{2} - U\int_{-\infty}^{\infty}\frac{d\omega}{2\pi}\frac{E_d}{D^{\mathrm{HF}}(i\omega)},$$
$$\delta = \sum_\alpha \Gamma_\alpha e^{i\Phi_\alpha} - U\int_{-\infty}^{\infty}\frac{d\omega}{2\pi}\frac{\delta + \sum_\alpha \Gamma_\alpha e^{i\Phi_\alpha}\left(\frac{\Delta_\alpha}{\sqrt{\Delta_\alpha^2+\omega^2}}-1\right)}{D^{\mathrm{HF}}(i\omega)}. \quad (11)$$

Close to the QPT, the inverse denominator $1/D^{\mathrm{HF}}(i\omega)$ is dominated by its zeros at the ABS energies $\pm\omega_0$ [i.e., $D^{\mathrm{HF}}(\pm\omega_0)=0$] which become zero at the QPT. Therefore, we may use the expansion of the determinant to the lowest (second) order in ω reading[2] as $D^{\mathrm{HF}}(i\omega) \approx E_d^2 + |\delta|^2 - [1+\sum_\alpha \Gamma_\alpha/\Delta_\alpha]^2 (i\omega)^2$ which gives us for the ABS energies close to the QPT $\omega_0 \approx \sqrt{E_d^2+|\delta|^2}/(1+\sum_\alpha \Gamma_\alpha/\Delta_\alpha)$. Obviously, the position of QPT coincides with the situation where $E_d = \delta = 0$. Close to the transition, the integrals are strongly dominated by the poles at $\pm\omega_0$ and we can approximately evaluate the first two leading contributions in inverse ABS energy (first of the order $1/\omega_0$ while the second of the order 1; all other terms are at least of order ω_0 and, thus, irrelevant at the transition) as follows:

$$\int_{-\infty}^{\infty}\frac{d\omega}{2\pi}\frac{1}{D^{\mathrm{HF}}(i\omega)} \approx \frac{1}{2\left(1+\sum_\alpha \Gamma_\alpha/\Delta_\alpha\right)^2}\int_{-\infty}^{\infty}\frac{d\omega}{\pi}\frac{1}{\left(\omega_0^2+\omega^2\right)} = \frac{1}{2\omega_0\left(1+\sum_\alpha \Gamma_\alpha/\Delta_\alpha\right)^2}, \quad (12a)$$

$$\int_{-\infty}^{\infty}\frac{d\omega}{2\pi}\frac{f(\omega^2)}{D^{\mathrm{HF}}(i\omega)} \approx \int_0^{\infty}\frac{d\omega}{\pi}\frac{f(\omega^2)}{D^{\mathrm{HF}}(i\omega)}\bigg|_{\omega_0=E_d=\delta=0} \quad (12b)$$

for a smooth function $f(x)$ vanishing at zero, i.e., $f(x\to 0)=0$. Using these approximations, we finally arrive at

$$E_d\left[1+\frac{U}{2\sqrt{E_d^2+|\delta|^2}\left(1+\sum_\alpha \Gamma_\alpha/\Delta_\alpha\right)}\right] = \varepsilon + \frac{U}{2},$$
$$\delta\left[1+\frac{U}{2\sqrt{E_d^2+|\delta|^2}\left(1+\sum_\alpha \Gamma_\alpha/\Delta_\alpha\right)}\right] = \sum_\alpha \Gamma_\alpha e^{i\Phi_\alpha} + U\mathcal{B}, \quad (13)$$

with $\mathcal{B}$ representing the band contribution

$$\mathcal{B} = \int_0^{\infty}\frac{d\omega}{\pi}\frac{\sum_\alpha \Gamma_\alpha e^{i\Phi_\alpha}\left(1-\frac{\Delta_\alpha}{\sqrt{\Delta_\alpha^2+\omega^2}}\right)}{\omega^2\left[1+\sum_\alpha \frac{\Gamma_\alpha}{\sqrt{\Delta_\alpha^2+\omega^2}}\right]^2 + \left|\sum_\alpha \Gamma_\alpha e^{i\Phi_\alpha}\left(\frac{\Delta_\alpha}{\sqrt{\Delta_\alpha^2+\omega^2}}-1\right)\right|^2}. \quad (14)$$

In Appendix A, we discuss the formula (14) in more detail in the symmetric case $\Delta_L = \Delta_R = \Delta$.

To obtain the phase boundary, we sum up squares of the two equations (13):

$$\left(E_d^2+|\delta|^2\right)\left[1+\frac{U}{2\sqrt{E_d^2+|\delta|^2}\left(1+\sum_\alpha \Gamma_\alpha/\Delta_\alpha\right)}\right]^2 = \left(\varepsilon+\frac{U}{2}\right)^2 + \left|\sum_{\alpha=L,R}\Gamma_\alpha e^{i\Phi_\alpha} + U\mathcal{B}\right|^2, \quad (15)$$

which yields at the phase boundary $E_d^2+|\delta|^2=0$ an implicit equation for the borderline

$$\frac{U^2}{4\left(1+\sum_\alpha \Gamma_\alpha/\Delta_\alpha\right)^2} = \left(\varepsilon+\frac{U}{2}\right)^2 + \left|\sum_{\alpha=L,R}\Gamma_\alpha e^{i\Phi_\alpha} + U\mathcal{B}\right|^2. \quad (16)$$

Omitting the band contribution $\mathcal{B}$ from Eq. (16) one gets a very simple approximation of the boundary called *generalized atomic limit* (GAL) [50]:

$$\frac{U^2}{4(1+\sum_\alpha \Gamma_\alpha/\Delta_\alpha)^2} = \left(\varepsilon+\frac{U}{2}\right)^2 + \Gamma_L^2 + \Gamma_R^2 + 2\Gamma_L\Gamma_R\cos(\Phi_L-\Phi_R). \quad (17)$$

Interestingly, as we show later on, at half-filling ($\varepsilon = -U/2$) the simple GAL boundary lies typically very close to the results obtained via the NRG method and/or the second-order perturbation expansion. This is not surprising since at half-filling the HF approximation reproduces the atomic limit exactly. Hence, one can expect that GAL, being a generalization of the atomic limit to noninteger occupation of the dot, delivers quite reliable results near the charge-symmetric state.

Furthermore, we may use Eq. (15) for finding $\sqrt{E_d^2+|\delta|^2}$ close to the phase boundary. Using the implicit-function theorem, we see that a solution with $\sqrt{E_d^2+|\delta|^2} > 0$ exists on one side of the boundary (moreover, the side containing the noninteracting $U\to 0$ limit, i.e., corresponding to the 0 phase) while $\sqrt{E_d^2+|\delta|^2} < 0$ on the other side. There, we must conclude, no solution to the restricted HF equations (13) exists, only when one allows for breaking of the spin symmetry (i.e., finite magnetization), which is however unphysical for a zero-dimensional impurity system, the appropriately extended

[2] See Appendix A for a more detailed discussion.

HF equations (10) do have a solution [41,44]. Since we do not want to resort to an unphysical symmetry breaking to obtain the π phase, we must conclude that the perturbative spin-symmetric solution breaks down at the phase boundary as expected from a general conceptual viewpoint [56]. Although these findings have been explicitly demonstrated on the level of the HF approximation, they are actually fully general and apply to any order of perturbation theory, in particular also to the second order which we are going to address now.

B. Second order: Dynamical corrections

It was shown in previous studies [50,51] that inclusion of dynamical corrections beyond the static HF into the self-energy can dramatically improve the quantitative predictions for both the position of the phase boundary and the physical quantities in the 0 phase. Already, first corrections from second order of the perturbation expansion were sufficient to reproduce fairly well the results of NRG in the case of identical leads. Second-order contributions to the self-energy read as

$$\Sigma^{(2)}(i\omega_n) = -\frac{U^2}{\beta}\sum_{\nu_m} G(i\omega_n + i\nu_m)\chi(i\nu_m) = \quad + \tag{18a}$$

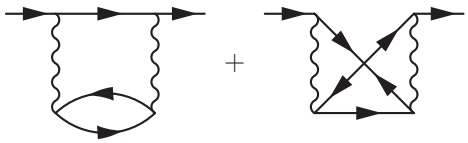

and

$$\mathcal{S}^{(2)}(i\omega_n) = -\frac{U^2}{\beta}\sum_{\nu_m} \mathcal{G}(i\omega_n + i\nu_m)\chi(i\nu_m) = \quad + \tag{18b}$$

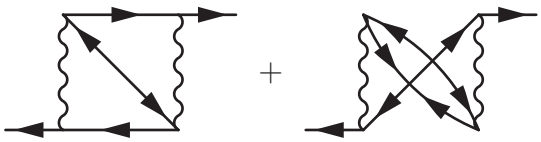

where

$$\begin{aligned}\chi(i\nu_m) &= \frac{1}{\beta}\sum_{\omega_k}[G(i\omega_k)G^*(-i\nu_m - i\omega_k) + \mathcal{G}(i\omega_k)\mathcal{G}^*(-i\nu_m - i\omega_k)] \\ &= \frac{1}{\beta}\sum_{\omega_k}[G(i\omega_k)G(i\nu_m + i\omega_k) + \mathcal{G}(i\nu_m + i\omega_k)\mathcal{G}^*(i\omega_k)] = \chi(-i\nu_m) = \chi^*(i\nu_m)\end{aligned} \tag{18c}$$

is the two-particle bubble consisting of the normal and anomalous parts and $\nu_m = 2\pi m/\beta$ is the mth bosonic Matsubara frequency. Analogously to the HF case before we can explicitly verify the charge-conservation condition (7); calculations are more tedious this time and we present them in Appendix B.

The Luttinger-Ward functional of this second-order correction to the Hartree-Fock approximation reads as

$$\begin{aligned}\phi^{(2)}[\widehat{G}] = -\frac{U^2}{2\beta^3}\sum_{\omega_n,\omega_k,\nu_m}&[G(i\omega_k)G^*(-i\omega_n)G(i\omega_n + i\nu_m)G^*(-i\omega_k - i\nu_m) + 2G(i\omega_k)G^*(-i\omega_n) \\ &\times\mathcal{G}(i\omega_n + i\nu_m)\mathcal{G}^*(-i\omega_k - i\nu_m) + \mathcal{G}(i\omega_k)\mathcal{G}^*(-i\omega_n)\mathcal{G}(i\omega_n + i\nu_m)\mathcal{G}^*(-i\omega_k - i\nu_m)]\end{aligned}$$

$$= \quad + \; 2 \quad + \quad . \tag{18d}$$

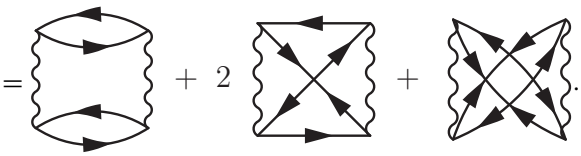

It is manifestly gauge invariant. These first two orders of the perturbation expansion are well controllable on the one-particle level. The higher contributions to the self-energy become more complex and their classification demands to introduce two-particle vertices as discussed in detail in Ref. [57]. Therefore, we resort just to the second order of the perturbation theory, which proves to be fully sufficient in the BCS-singlet regime for weak and intermediate coupling. The second-order self-energy corrections (together with the first-order HF counterparts) are inserted into Eq. (4) to obtain a self-consistent nonlinear functional equation for the Green function as a function of frequency. Unlike the HF case, the resulting equations for the Green function components defy analytical treatment and must be solved numerically. In the following, we refer to this approach as the *full self-consistent dynamical correction* (FDC) approximation.

As discussed previously for the symmetric leads [50], nearly identical results can be obtained in the weak coupling regime by evaluating the dynamical self-energies (18) using just the fully converged self-consistent HF solution as the input into the Green function (DC approximation). The DC approach can be represented by the following algorithm:

(1) Compute the HF Green function as described in Sec. III A.

(2) Compute the second-order contributions to self-energy $\Sigma^{(2)}(i\omega_n)$ and $\mathcal{S}^{(2)}(i\omega_n)$ using formulas (18) with $G^{\mathrm{HF}}(i\omega_n)$ and $\mathcal{G}^{\mathrm{HF}}(i\omega_n)$ instead of $G(i\omega_n)$ and $\mathcal{G}(i\omega_n)$. These second-order contributions stay fixed throughout further calculations.

(3) Compute the DC self-energies $\Sigma^{\mathrm{DC}}(i\omega_n) = \Sigma^{(1)} + \Sigma^{(2)}(i\omega_n)$ and $\mathcal{S}^{\mathrm{DC}}(i\omega_n) = \mathcal{S}^{(1)} + \mathcal{S}^{(2)}(i\omega_n)$ with $\Sigma^{(1)} = \Sigma^{\mathrm{HF}}$ and $\mathcal{S}^{(1)} = \mathcal{S}^{\mathrm{HF}}$ in the first iteration.

(4) Compute the DC Green function $\widehat{G}^{\mathrm{DC}}(i\omega_n)$ using definitions (4) and (5) with $\Sigma(i\omega_n) = \Sigma^{\mathrm{DC}}(i\omega_n)$ and $\mathcal{S}(i\omega_n) = \mathcal{S}^{\mathrm{DC}}(i\omega_n)$.

(5) Compute the first-order contributions to self-energies: $\Sigma^{(1)} = \frac{U}{\beta}\sum_{\omega_n} G^{\mathrm{DC}}(i\omega_n)e^{i\omega_n 0^+}$ and $\mathcal{S}^{(1)} = \frac{U}{\beta}\sum_{\omega_n} \mathcal{G}^{\mathrm{DC}}(i\omega_n)$.

(6) Repeat steps 3 to 5 until the convergence criterion of the self-consistency is achieved.

The algorithm implies that the convolutions in the second-order self-energies are evaluated just at the beginning of the procedure. The fixed dynamical self-energies are then used to calculate self-consistently the first-order contributions to the self-energies.

Note that the DC approximation is numerically more stable close to the phase transition than the FDC approximation (see Fig. 2). In addition, it allows us to study the intermediate coupling regimes, where full self-consistent approaches often fail to give physically correct solution. It is fairly well known that the fully self-consistent second-order approximation as well as its extensions via sums of ladders and chains fail for intermediate coupling of impurity models. They not only smear the Hubbard satellite bands [58], they also miss the Kondo physics [59]. That is why simplified self-consistencies often provide better approximations than the fully self-consistent ones [60].

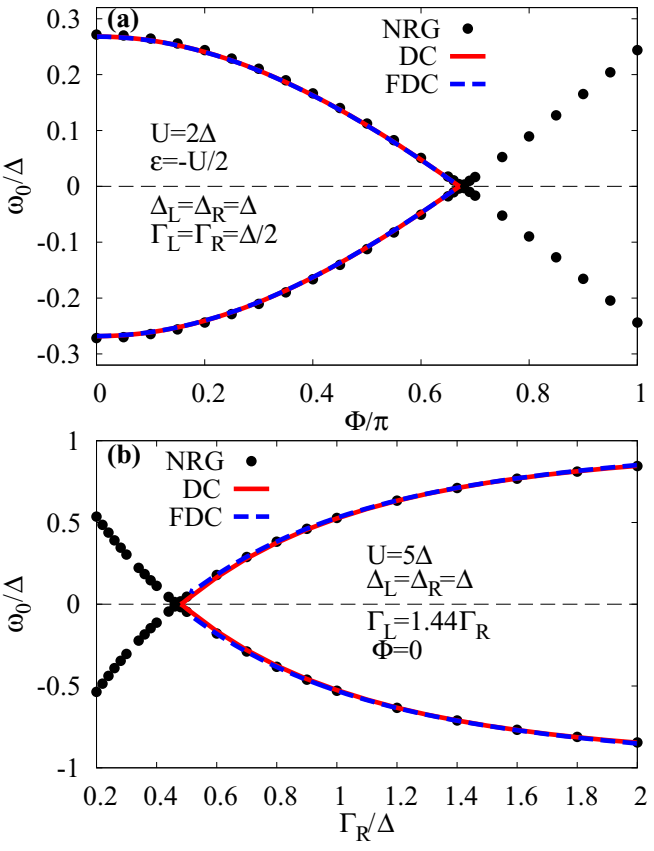

FIG. 2. Andreev bound-state energies dependence on the phase difference Φ for the symmetric coupling $\Gamma_L = \Gamma_R$ (a) and on the coupling Γ_R for asymmetric coupling $\Gamma_L = 1.44\Gamma_R$ at $\Phi = 0$ (b). The solid lines were calculated via the DC approximation, the dashed lines via the FDC approximation, and the bullets were obtained using NRG with $\Lambda = 4$. The point where bound and antibonding states merge/cross at the Fermi level (zero energy) is identified with the 0-π quantum phase transition.

IV. RESULTS AND DISCUSSION

We provide a comparison of the ground-state, i.e., zero-temperature, results obtained via the perturbative method discussed above with those obtained using the NRG approach which is a reliable nonperturbative numerical method for the ground-state properties [61]. For NRG calculations we used the NRG LJUBLJANA open source code [52,53] mostly with the logarithmic discretization parameter Λ set to the value of 4 as is common for double-channel problems. We also tested and used other values of Λ [see Fig. 4(a)] and found out that for most of the studied cases, the phase boundary is not sensitive to Λ. This is in compliance with the findings discussed in Ref. [38].

Various theoretical studies showed that the 0-π phase transition, where the supercurrent changes its sign, is accompanied by a smooth crossing of the Andreev bound states [21,32,40,43,45] which is in agreement with the experiments [3,18,21]. Although the perturbation approach without spin-symmetry breaking can not be easily extended into the π phase and, therefore, does not show the actual crossing of the ABS [50], the ABS smoothly reach the Fermi energy at the border of the 0 phase [50,51]. In Fig. 2 we plot examples of the ABS dependencies on the phase difference Φ for symmetric coupling $\Gamma_L = \Gamma_R$ [Fig. 2(a)] as well as on the right coupling Γ_R for asymmetric coupling $\Gamma_L = 1.44\Gamma_R$ [Fig. 2(b)]. We identify the point where both (bound and antibonding) ABS reach the Fermi energy with the boundary of the 0 phase, i.e., with the point of the quantum phase transition. This is fully supported by the NRG data. It can be seen in Fig. 2 that the crossing of the ABS obtained by the NRG (bullets) coincides with the merger of the ABS obtained via the DC approximation (solid red lines). The dashed blue lines in Fig. 2 were obtained via the FDC approximation. One can see that the FDC and DC results practically coincide in both presented cases apart from the very close neighborhood of the phase transition, where the FDC becomes numerically unstable.

It should be stressed that analytic continuation of the Matsubara formalism to the real frequencies is necessary for the study of ABS. This usually leads to quite complicated formulas for the Green functions [51], however, sometimes this approach is numerically more stable than the Matsubara formalism. Nevertheless, the continuation to the real axis can be avoided if one is interested only in the phase boundaries. The determinant $D(i\omega_n)$ yields zero at the phase transition point exactly for $i\omega_n = 0$. Therefore, one can use the smooth dependency of $D(0)$ on different model parameters for the direct estimation of the phase boundary.

A. Phase diagrams for $\Delta_L = \Delta_R$

Setups where $\Delta_L = \Delta_R \equiv \Delta$ in practice mean that both leads are made of the same material. Since this is a common situation in the experiment, this case has been intensively studied [25]. We start our discussion with three phase diagrams known from the literature [38]. The main reason for this is to show that the simple second-order expansion theory is sufficient for a broad range of parameters and even in the regimes where usually much more elaborated techniques are used. Simultaneously, we compare the results of the three approximations, namely, HF, DC, and GAL and discuss their limitations.

In Fig. 3(a), we plot the ground-state phase diagrams in the Γ_R-U plane for $\Phi = 0$ and π at half-filling ($\varepsilon = -U/2$). The left-right lead asymmetry is fixed by the coupling ratio $\Gamma_L = 1.44\Gamma_R$. The first thing that should be noticed is that the HF approximation without broken spin symmetry yields a qualitatively correct description of the phase boundary at half-filling. However, its phase-boundary curve is close to the NRG border only for small Coulomb interaction ($U \lesssim 2\Delta$). A much better result is obtained by using its simplification, namely, the GAL approximation, which neglects the band contribution. This implies that the HF approximation overestimates the contribution from the bands. Considering its simplicity, the GAL method provides a very good and fast approximation of the phase boundary at half-filling even for $U \gg \Delta$. Nevertheless, regarding the accuracy it is overperformed by the DC approximation. One can see that the DC border reproduces the NRG data (for $\Lambda = 4$) almost perfectly. This shows that the perturbation theory with the simplest dynamical corrections can lead to a correct estimation of the quantum phase boundary for the studied system. This statement is true not only for the symmetric-leads case studied in Ref. [50], but also for the experimentally more relevant setups.

A similar agreement between the DC and NRG phase boundaries can be seen in Fig. 3(b), where the phase diagrams are plotted away from half-filling at $\varepsilon = -2.5\Delta$. On the other hand, the bias of the level energy ε strongly influences both the HF and GAL curves. The GAL border approaches the NRG data only around $U = 5\Delta$, i.e., just near the half-filling occupation. The HF border is way off in the whole plotted range. In addition, both HF and GAL results drift away from the DC and NRG border with the increasing U. Because of the structure of Eq. (16), the GAL and HF borders approach each other for $U \to 0$, where the term $U\mathcal{B}$ vanishes, as well as for $|\epsilon + U/2| \gg \Delta$ where the first term dominates the right-hand side of Eq. (16). The latter one can be seen in Fig. 3(c). Here, we plot the phase diagram in the Γ_R-ε plane for moderately large Coulomb interaction $U = 5\Delta$ and two values of Φ. The HF and GAL borders coincide far away from half-filling for both values of Φ. As before, despite its simplicity, both these approximations yield a fair qualitative agreement with the NRG data. However, with the exception of the GAL curve near the half-filling, both approximations fail to reproduce the NRG data quantitatively. In contrast, the DC border matches the NRG in a broad region around $\varepsilon = -U/2$ and even outside this region the difference between NRG data and DC curve is much smaller than Δ. This shows that the proper treatment of the frequency dependence of the correlation effects is crucial for the quantitative description of the 0-π transition.

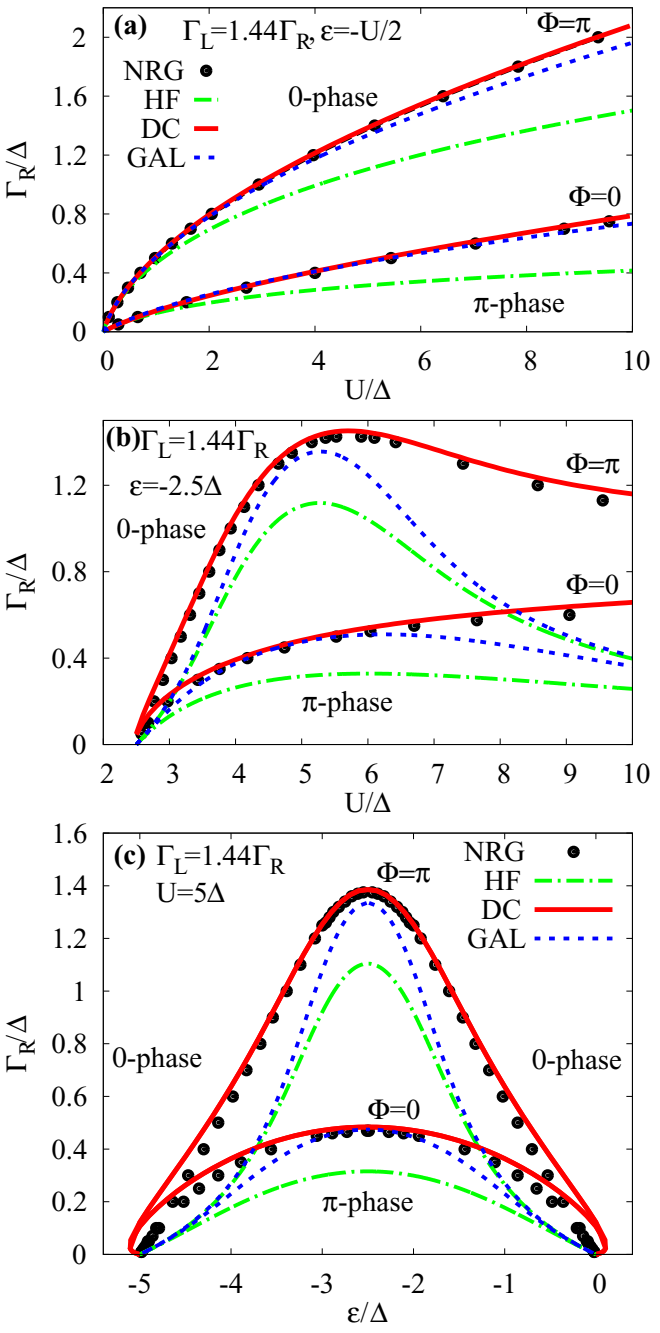

FIG. 3. Phase diagrams in the Γ_R-U plane at the half-filling (a), and for $\varepsilon = -2.5\Delta$ (b) and in the Γ-ε plane for $U = 5\Delta$ (c). We compare the phase boundaries calculated by NRG with the spin-symmetric HF, the second-order PT/dynamical corrections (DC), and generalized atomic limit approximation (GAL).

The most evident (qualitative) discrepancy of the DC curve from the NRG are the "humps" at the bottom of the phase diagrams Figs. 3(c) and 4(a). This is not surprising as here $U \gg \Gamma$ and therefore we are on the edge of the usability of the perturbation expansion in U (see Fig. 1). On the other hand, these humps resemble a formation of the islandlike phase diagram known from the previous NRG study by Oguri *et al.* [40]. They showed that in case of strongly asymmetric gaps $\Delta_L \gg \Delta_R$ and decreasing U, a reentrant doublet region

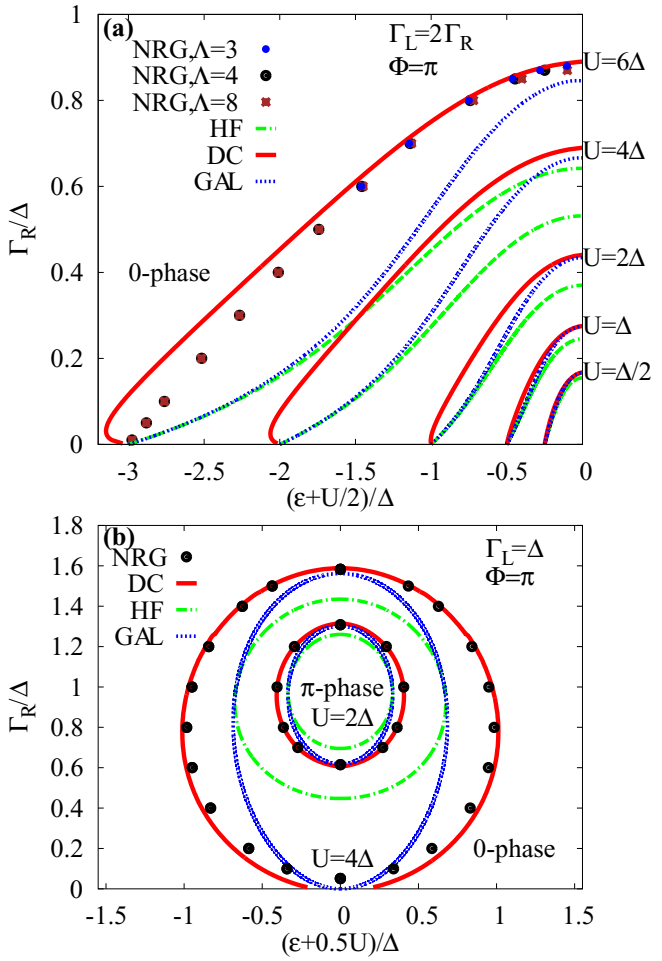

FIG. 4. Phase diagrams in the Γ_R-ε plane for different values of U, $\Phi = \pi$ and asymmetric leads $\Gamma_L = 2\Gamma_R$ (fixed ratio) (a) and $\Gamma_L = \Delta$ (varying ratio Γ_R/Γ_L which induces the π-phase island structure) (b).

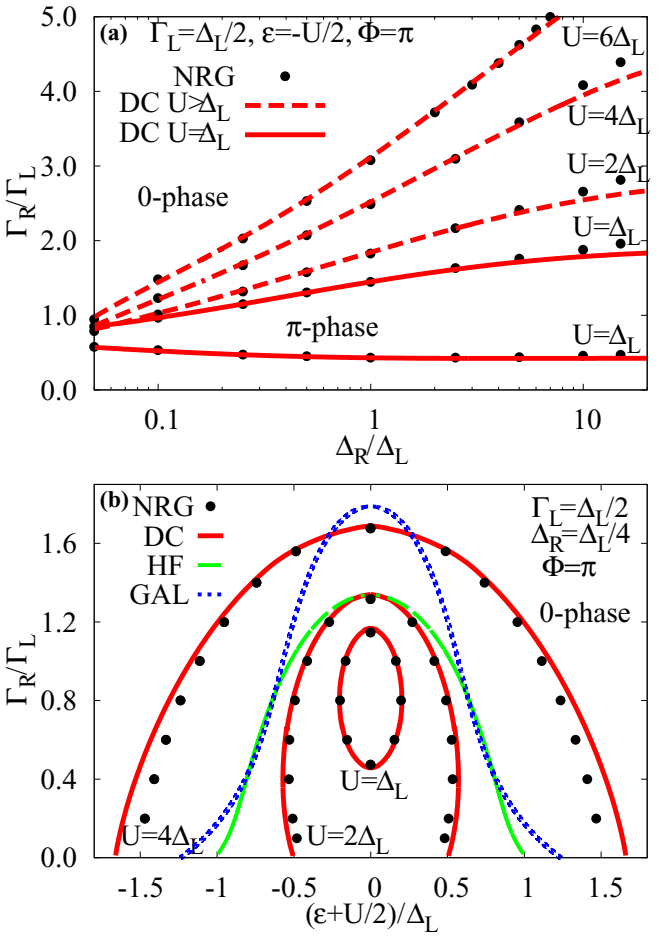

FIG. 5. (a) Critical tunnel-coupling ratio Γ_R/Γ_L as a function of SC-gap ratio Δ_R/Δ_L for $\Gamma_L = \Delta_L/2$, $\Phi = \pi$ at half-filling. (b) Phase diagrams in the Γ_R/Γ_L-ε plane with asymmetric lead SC gaps $\Delta_R = \Delta_L/4$ calculated via NRG and DC approximation for $U/\Delta_L = 1,2,4$ and compared for $U = 4\Delta_L$ with HF and GAL approximations.

appears as an island in the Γ_R-ε plane (see Fig. 12 in Ref. [40]). However, this is not the case in Fig. 4(a). For the fixed ratio Γ_L/Γ_R and $\Delta_L = \Delta_R$, the humps are only a consequence of the perturbative treatment. Unlike in Ref. [40] they are obviously disappearing with the decreasing U [Fig. 4(a)] and no island structure appears even for $U = \Delta/2$. Nevertheless, the situation is different if one varies the ratio Γ_L/Γ_R. In Fig. 4(b), we show that the condition $\Delta_L \gg \Delta_R$ used by Oguri *et al.* is not necessary for obtaining the island structures of the π phase. All three approximations show these structures when the ratio Γ_L/Γ_R is varied. Nevertheless, as before, only the DC approximation matches quantitatively with the NRG outside the half-filling for plotted values of U.

Because we have observed this behavior also for other values of Γ_L/Δ [for another example, see the reentrant behavior at $\Delta_R/\Delta_L = 1$ for $U = \Delta_L$ lines in Fig. 5(a)], we conclude that the island structures are primarily a function of the difference between the hybridizations Γ_L and Γ_R. In general, the π phase is destabilized by the increasing differences between the couplings. As this can be in principle tuned in the experiment [1], one can expect that the island structures can be verified experimentally. Regarding the U dependence, one can see that the increasing Coulomb interaction inflates the π-phase area in both panels of Fig. 4.

We use Fig. 4(a) to demonstrate two technicalities. First, it is an illustrative way to show that all three approximations converge to each other with decreasing U as it should be. All borders practically coincide for the lowest $U = \Delta/2$. Second, we present a test of the NRG for the largest value of Coulomb interaction $U = 6\Delta$ corresponding to the most correlated case. There is only a very weak dependence of the NRG phase boundary on the parameter Λ which makes the generic calculations at $\Lambda = 4$ highly reliable.

B. Phase diagrams for $\Delta_L \neq \Delta_R$

Significantly less attention has been paid, both experimentally and theoretically, to the general case $\Delta_L \neq \Delta_R$ than to the identical leads $\Delta_L = \Delta_R$. This can change in the near future as a recent experiment on a carbon nanotube quantum dot coupled to Nb fork and Al tunnel probe [22] not only showed that such a setup is technically possible, but in addition it revealed a nontrivial formation of ABS. Theoretical efforts so far have been, however, mainly focused on the $\Delta_L = \Delta_R$ case

despite the fact that previous theoretical studies dealing with some special cases of nonidentical leads showed that the lead difference can strongly affect the quantum phase transition [38,40].

We demonstrate this for a wide range of ratios Δ_R/Δ_L in Fig. 5(a). Here, the phase boundary obtained via the DC approximation and NRG is plotted in the Γ_R/Γ_L-Δ_R/Δ_L plane for various values of U at half-filling. We have set the coupling to the left lead to $\Gamma_L = \Delta_L/2$ and the phase difference to $\Phi = \pi$. One can see that the DC curves are in excellent agreement with the NRG results in the plotted range of Δ_R/Δ_L which spans two orders of magnitude (note the logarithmic horizontal scale). This once again proves the reliability of the DC approximation also for unequal gaps in the leads.

We can observe two different kinds of phase diagrams in Fig. 5(a). Two phase boundaries separating the 0 and π phases are present for $U = \Delta_L$ (solid curves), but only a single phase boundary is realized in the plotted region for $U \geqslant 2\Delta_L$ (dashed curves). This is in compliance with the study of $\Delta_R \gg \Delta_L$ case in Ref. [40] as well as with the opening of island structures as a consequence of increasing U observed in the phase diagrams plotted in Figs. 4(b) and 5(b).

Oguri *et al.* [40] showed that in the limit $\Delta_R \to \infty$ the model (1a) can be mapped onto a single-channel model where the right lead is replaced by an onsite superconducting gap at the impurity, i.e., the standard superconducting atomic limit [35,37] performed for the right lead only. Our observation that the critical Γ_R depends only weakly on the ratio Δ_R/Δ_L for the large right gap and weak Coulomb interaction [see $U = \Delta_L$ boundaries in Fig. 5(a)] justifies applicability of this simplified model.

The GAL and HF phase boundaries are in a fair qualitative agreement with DC and NRG even for $\Delta_L \neq \Delta_R$ case. Nevertheless, both these simple approximations fail quantitatively in positioning the critical curves in the phase diagram. This can be seen in Fig. 5(b) where the 0-phase boundaries are plotted in the Γ_R/Γ_L-ε plane for $\Delta_R = \Delta_L/4$ and $\Gamma_R = \Gamma_L/2$. On the other hand, the DC approximation largely coincides with NRG even for $U = 4\Delta_L$ and fully reproduces the π-phase island structure obtained with NRG for $U = \Delta_L$.

C. Applicability and limitations of the method

Despite its reliability in a wide range of the input parameters, the present method has natural application limits. We can roughly divide them into two classes. The first one is related to the very conceptual foundation of the method in the (resummed) perturbation theory which implies its breakdown at the quantum phase transition and impossibility to reach the π phase with the doubly degenerate ground state. Any quantities in the π phase are presently inaccessible by our approach. The impossibility to take into account the π phase has a serious consequence in that the method cannot address nonzero temperatures. At nonzero temperatures, both the 0 and π phases coexist and this coexistence results in a temperature-smoothened behavior of all quantities around the transition. This is, however, completely neglected in the present perturbative treatment that is built upon only the singlet equilibrium state, 0 phase, even if it becomes metastable (at nonzero temperature) and should actually be replaced by the spin doublet, π phase. Mixing of the singlet and doublet states is relevant only in a close vicinity of the phase transition since far away from it the physics is still described well by either of the states. Yet, this conceptual limitation is serious, especially since there is no clear way how to circumvent it. There is, however, a perturbative expansion for elementary excitations and Green functions in systems with a degenerate equilibrium state [62].

The second class of limitations concerns the standard fact that perturbation methods have limited range of applicability given by the level of sophistication of the included perturbation contributions. Such theories typically do not explicitly break down but they become quantitatively highly imprecise and eventually useless. Our approach is conceptually meaningful in the 0 phase and can be used not only for determination of the position of 0-π phase boundaries, but also for calculation of various (single-particle) quantities such as the Josephson current, QD occupation, proximity-induced local gap, energies of ABS, etc. [50,51]. Since it is a perturbation expansion in the Coulomb interaction truncated at the lowest-order diagrams, it is clear that it ceases to be reliable for large enough U. This can happen in various ways depending on the values of the other model parameters Δ, Γ, and ε. We have already encountered such a situation in Figs. 3(c) and 4(a) where there was an obvious discrepancy (although not too severe) for small Γ close to charge-degeneracy points. Small Γ effectively increases the importance of the Coulomb interaction via the increased ratio U/Γ, pushing the system close to the atomic limit, where the complementary perturbation expansion in Γ is a more suitable choice [28,34].

For decreasing Γ and fixed Δ, the perturbation expansion around the atomic limit works fine, but if one allows also the SC gap Δ to decrease comparably to the (normal-state) Kondo temperature $T_K \sim \sqrt{\frac{U\Gamma}{2}} \exp\left[\pi \frac{\varepsilon}{2\Gamma}(1 + \frac{\varepsilon}{U})\right]$, the system enters into a strongly correlated Kondo state where any simple perturbation theory inevitably fails. We demonstrate this crossover from the conventional BCS singlet to the Kondo singlet [37] and gradual failure of the DC approximation in Figs. 6 and 7 for symmetric leads at half-filling. In Fig. 6, we present the phase diagram in the Δ-U plane studied previously in the literature using different methods including the NRG [37] and the expansion around the atomic limit (for Δ much larger than the characteristic energies of the dot) based on the self-consistent description of the Andreev bound states (SC ABS) [36]. We compare the phase boundaries obtained via these methods with the DC and GAL boundaries in Fig. 6. Note, that the DC approximation is so good that we had to use the logarithmic scale for the Δ axis to visualize deviations of the DC boundary from the NRG data. The DC boundary departs from the NRG points for $\Delta/\pi\Gamma \lesssim 0.03$, nevertheless, even in this parameter range the DC boundary is still much closer to the NRG boundary than the SC ABS curve, which can be attributed to the violation of the large-Δ assumption inherent to the SC ABS approach. However, the GAL branches off from NRG points significantly with decreasing Δ.

The horizontal arrows in Fig. 6 correspond to the values of the gap for which the one-particle quantities are plotted in Figs. 7(a) (ABS energies ω_0) and 7(b) (proximity-induced local

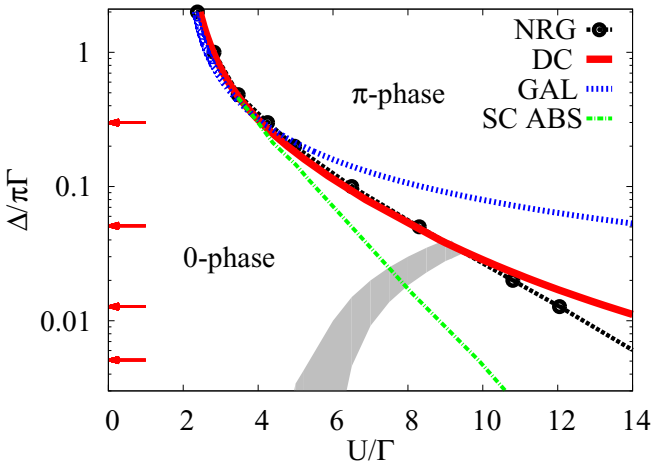

FIG. 6. Phase diagram in the Δ-U plane for $\phi = 0$. NRG solution (black bullets connected by dashed lines) is compared with the DC approximation (red full line), GAL (blue dotted line), and the SC ABS method taken graphically from Fig. 3 in Ref. [36] (green dotted-dashed line). Notice the logarithmic scale on the vertical Δ axis, where the arrows point out the values of the gap used for curves plotted in Fig. 7. The gray stripe marks the region where DC results start to depart from the NRG in Fig. 7, i.e., the position of the crossover from the BCS to the Kondo singlet ground state.

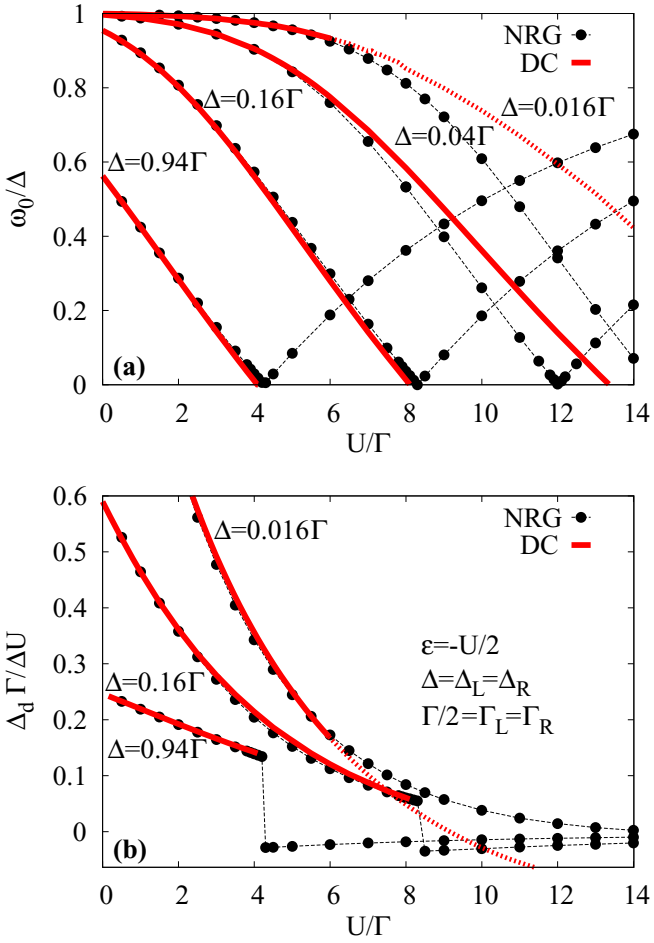

FIG. 7. Limitations of the DC approximation: comparison of the NRG (bullets) and DC approximation (solid lines) results for symmetric setups at half-filling. Interaction strength U dependence of the ABS energies (a) and scaled proximity-induced gap $\Delta_d = U\langle d_\uparrow d_\downarrow\rangle$ (b) for the four values of the gap Δ shown by arrows in Fig. 6 and taken from Ref. [37] (the curve for $\Delta = 0.04\Gamma$ was omitted in the lower panel just for its readability). The breakdown of the DC method can be seen for large interaction U/Γ and small SC gap Δ as indicated in Fig. 6. The dashed part of the $\Delta = 0.016\Gamma$ lines is numerically unstable.

gap $\Delta_d = U\langle d_\uparrow d_\downarrow\rangle$; the curve $\Delta = 0.04\Gamma$ is not displayed just for clarity). There is almost a perfect agreement between DC and NRG curves for $\Delta/\Gamma > 0.1$ in the entire 0 phase. For smaller values of Δ and sufficiently large U, both ABS energies and Δ_d obtained using the DC approximation depart from the NRG points with increasing ratio U/Γ and can even become numerically unstable (dashed lines). We estimated the region where the DC curves start to deviate significantly from the NRG by the gray stripe in Fig. 6. We consider this to be the crossover region between the BCS and Kondo singlet ground states and, therefore, also the edge of applicability of the DC approximation. As we will show in the next section, this edge still leaves plenty of space for the second-order expansion in U to be the method of choice for the description of real systems.

In Appendix B, we have proven that the FDC approximation is charge conserving in the general case and that DC approximation is charge conserving for the experimentally generic case of equivalent gaps. The charge conservation for the DC unfortunately does not extend to the general case, giving it the same status as the conventional implementation of fRG [46]. In Fig. 8, we compare the numerical results obtained by these two methods with the NRG. The supercurrents at the left/right junctions are plotted as functions of ε for $U = \Delta_L$, $\Phi = \pi/2$, $\Gamma_L = 2\Gamma_R = \Delta_L/2$ and three values of Δ_R/Δ_L. We used the FDC approximation to calculate the supercurrent for $\varepsilon + U/2 < 0$ and the DC approximation for $\varepsilon + U/2 \geqslant 0$. It can be seen that both approaches are in excellent agreement with the NRG. However, only the FDC approximation fully conserves the current in the general case $\Delta_L \neq \Delta_R$. This is shown in the insets of Fig. 8 where the details of the current are plotted close to half-filling. The DC approximation conserves current for $\Delta_L = \Delta_R$ but not for $\Delta_L \neq \Delta_R$ as illustrated in the right inset. The difference between J_L and $-J_R$ is nevertheless very small, below 1% for the used parameters (see the vertical J-axis scale in the inset), which justifies the widespread usage of the DC approximation in this work as a faster and numerically more stable (especially around the phase boundary) alternative to the FDC approximation, which still gives trustworthy results even for $\Delta_L \neq \Delta_R$.

Finally, we mention yet another aspect of the DC method, which is its ability to calculate also spectral functions. This is possible by making use of analytic continuation of the Matsubara formalism to the real frequencies as shown in Refs. [50,51,57]. Here, we just plot the typical normal and anomalous spectral densities for the asymmetric coupling to the leads calculated using the DC approximation (solid red line), FDC approximation (dashed-dotted blue line), and NRG (dashed black line) in Fig. 9. Discretization parameter $\Lambda = 4$ and the logarithmic-exponential broadening of the data with the broadening parameter $b = 0.15$ together with the z trick

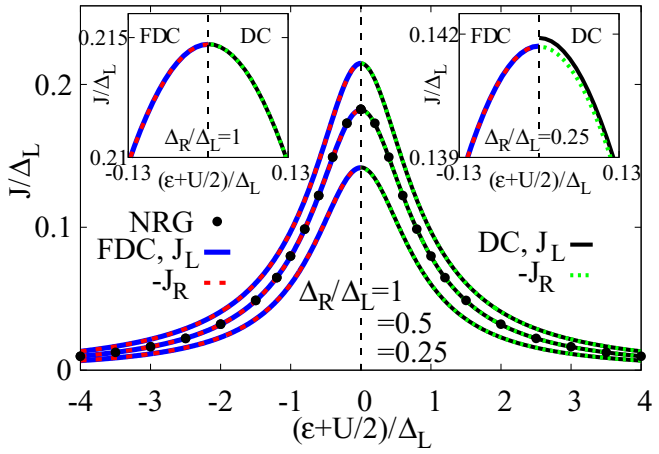

FIG. 8. Supercurrent through the left/right junctions as a function of ε for $U = \Delta_L$, $\Phi = \pi/2$, $\Gamma_L = 2\Gamma_R = \Delta_L/2$, and $\Delta_R/\Delta_L = 1, \frac{1}{2}, \frac{1}{4}$. The current was calculated using the FDC approximation for $\varepsilon + U/2 < 0$ and DC approximation for $\varepsilon + U/2 \geqslant 0$. The insets show details close to the half-filling.

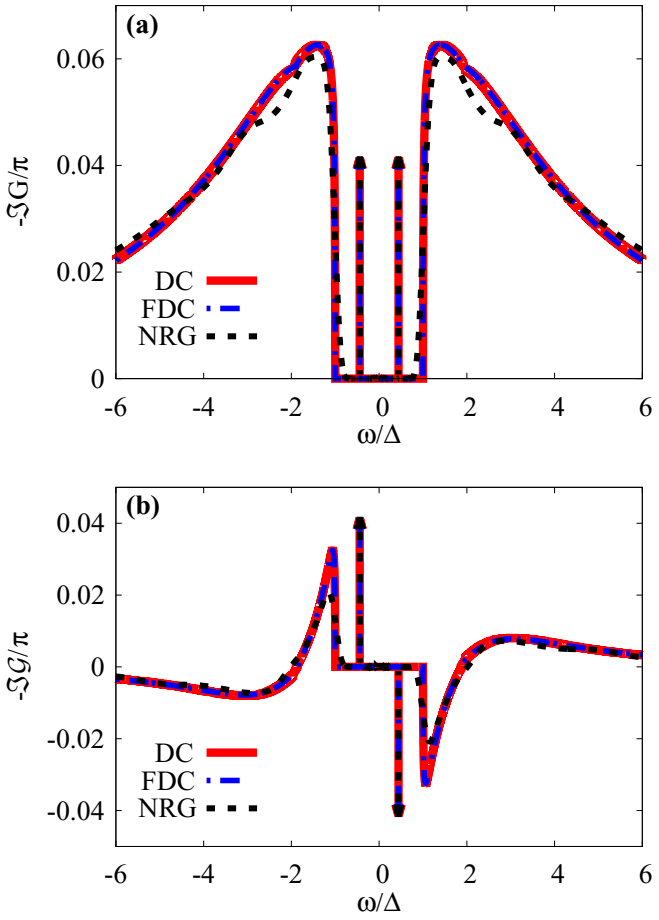

FIG. 9. Normal $-\mathrm{Im}G/\pi$ (a) and anomalous $-\mathrm{Im}\mathcal{G}/\pi$ (b) spectral densities for $U = 4\Delta$, $\Gamma_R = \Delta$, $\Gamma_L = 2\Gamma_R$ (asymmetric coupling), $\Phi = \pi/2$, and $\varepsilon = -U/2$ (half-filling) calculated using the DC approximation (red solid line), FDC approximation (blue dashed-dotted line), and NRG (black dashed line). Discrete Andreev bound states within the gap are represented by arrows whose height is determined by their weight.

(see the manual to Ref. [52]) was used for the NRG plot. Considering the simplicity of the (F)DC approximations and the broadening of NRG curves, which is fully responsible for the discrepancies around the band edge, the spectral functions are in a very good agreement, notice especially the perfect agreement both in the position and weight of the ABS.

V. COMPARISON WITH EXPERIMENTS

A. Grenoble experiment [Phys. Rev. X 2, 011009 (2012)]

Realization of a fully tunable superconducting carbon-nanotube quantum dot SQUID by Maurand *et al.* [20] allowed to determine the phase diagram for the 0-π phase transition in the Γ-ε plane experimentally (Fig. 10). In the experiment, the Coulomb interaction was measured from the finite-bias spectroscopy of the Coulomb-blockade diamonds and estimated to be $U = 0.80 \pm 0.05$ meV. The superconducting gap $\Delta \approx 0.08$ meV was determined from the peaks in the nonequilibrium (finite-bias) differential conductance. The analysis of the maximum of normal-state conductance showed that the tunneling amplitudes to the leads were balanced; therefore, the symmetric setup ($\Gamma/2 = \Gamma_L = \Gamma_R$) was assumed. Hybridization Γ for different tunings of the setup was estimated from the half-width at half-maximum of the Kondo resonance in the finite-bias conductance. The authors argue that the Kondo screening plays a key role for the 0-π phase transition in their device. This statement is supported by a quantitative comparison of the position of phase boundary with their theoretical predictions based on the SC ABS approximation [36], which is a perturbative method based on the superconducting atomic limit [35,37] with expansion for finite gap Δ. The key role of the Kondo screening is emphasized also from the identified operating regime of the experiment marked in Fig. 7 of Ref. [20]. Considering this and the limitations of the DC approach discussed above, it is

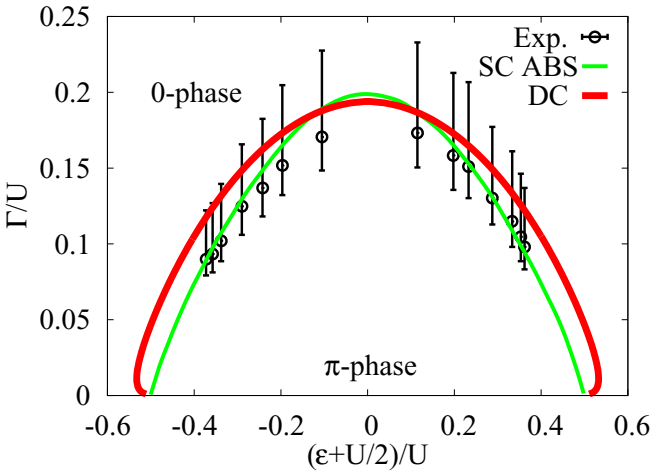

FIG. 10. Phase boundary between 0 and π phases as a function of ε and Γ/U. Both the experimental data (with the estimated Coulomb repulsion $U = 0.8$ meV and SC gap $\Delta = 0.08$ meV) and the theoretical curve calculated using the self-consistent description of Andreev bound states (SC ABS) [36] were taken graphically from Fig. 6 of Ref. [20]. The DC phase boundary was calculated for $U/\Delta = 10$ and $\Phi = 0$.

surprising that the actual DC phase boundary calculated for the same parameters as SC ABS ($U/\Delta = 10$) is very close to the experimental one as shown in Fig. 10. Although the SC ABS phase boundary is closer to experimental points than the DC boundary, that is still within the experimental error bars. Therefore, we conclude that the DC method performs well even beyond its expected validity range and can be applied to a very broad range of real superconducting quantum dots.

B. Orsay experiment [Phys. Rev. B 91, 241401(R) (2015)]

The most recent experimental study [23] of the superconducting carbon-nanotube quantum dot confirmed theoretical predictions that the 0-π phase transition can be controlled not only by the gate voltage, but also by the superconducting phase difference Φ tuned by the magnetic flux piercing the SQUID loop with the carbon-nanotube Josephson junction. The superconducting gap of the leads $\Delta = 0.17$ meV and the Coulomb interaction $U = 3.2$ meV, both with uncertainty $\sim$10%, were experimentally determined by standard methods (see the previous subsection). Total hybridization $\Gamma = \Gamma_R + \Gamma_L = 0.44$ meV and the asymmetry $\Gamma_R/\Gamma_L = 4$ of the couplings were obtained by comparing the measured normal-state finite-temperature linear conductance with the one obtained from CT-INT quantum Monte Carlo [43] calculations for the Anderson impurity model analogously to Ref. [26]. The experimental results were compared to QMC calculations and an excellent agreement was observed both for the current-phase relation as well as for the shape and width of the 0-π boundary in the Φ-ε plane. However, a shift of the energy level $\delta\varepsilon = 0.28$ meV of unknown origin was needed to overlap the experimental data with the theoretical curve.

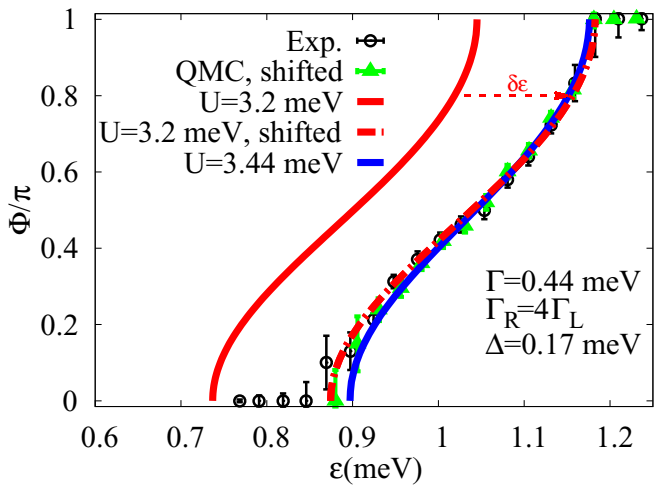

FIG. 11. Comparison of phase boundary in the Φ-ε plane obtained experimentally with different theoretical predictions. Both the experimental data and QMC points were taken graphically from Fig. 4(b) in Ref. [23]. Experimentally determined parameters (for details see the main text) $\Delta = 0.17$ meV, $U = 3.2$ meV, $\Gamma = \Gamma_R + \Gamma_L = 0.44$ meV, and $\Gamma_R/\Gamma_L = 4$ are subject to roughly 10% uncertainty. According to Ref. [23], the QMC curve was horizontally shifted to match the experiment. We plot the DC approximation for $U = 3.2$ meV (solid red curve), the same result shifted by $\delta\varepsilon$ to overlap the experiment (dashed red curve), and result for $U = 3.44$ meV within the experimental uncertainty without any further modification (blue full line).

In Fig. 11, we have calculated the 0-phase boundary with the DC approximation (solid red line) and compared it with the experimental and QMC data taken graphically from Fig. 4(b) in Ref. [23]. One can see that after introducing a small shift $\delta\varepsilon = 0.14$ meV, exactly as it was done for the QMC results, the simple second-order perturbation theory reproduces (the shape and width of) the phase boundary almost perfectly (dashed-dotted red curve in Fig. 11). We have taken the advantages of the DC approximation (its simplicity and speed) to check how the boundary depends on the variance of used parameters. We have found out that although the shape and width of the boundary are quite robust within the 10% uncertainty, the ε position of the boundary is very sensitive to the value of U. No shift of the phase boundary is needed if the value $U = 3.44$ meV within the U uncertainty range is used instead as it is shown in Fig. 11 (blue solid curve). This leads us to the conclusion that the deviations between theory and experiment observed in Ref. [23] are within the experimental uncertainty. Moreover, this is yet another demonstration of the usefulness of the DC approach for real systems.

VI. CONCLUSIONS

To summarize, we presented a detailed study of the self-consistent second-order perturbation expansion in the interaction strength of the superconducting single-impurity Anderson model. Based on a thorough analysis of its properties, we showed that it can reliably substitute time and resources consuming numerical methods such us the NRG or QMC for the study of the 0-π phase transitions and properties of the 0 phase in superconducting quantum dots for a broad range of parameters. It can be the method of first choice for realistic setups with asymmetric tunnel couplings and even for unconventional setups with different SC leads. We disclosed its big potential by successful fits of two existing experimental data sets for the 0-π phase boundary, including the suggestion for a plausible explanation of the existing discrepancy between the newest experiment and corresponding QMC results.

The approach can be straightforwardly applied to any single-particle quantity in the 0 phase such as supercurrent, local occupation and proximity-induced superconducting gap, or energies and weights of the Andreev bound states including the position of the 0-π quantum phase boundary at zero temperature. Due to its perturbation-theory roots it, however, conceptually fails in the description of the π phase and, consequently, also in the description of the finite-temperature properties close to the phase boundary. A possible remedy of the perturbation approach to reach also the π phase with the doublet ground state remains an open challenge, which in view of the successes of the method in the 0 phase is worth taking up in future studies.

ACKNOWLEDGMENTS

This work was supported by Grant No. 15-08740Y of the Czech Science Foundation (M.Ž.) and by the National Science Centre (Poland) under the Contract

No. DEC-2014/13/B/ST3/04451 (T.N.). V.J. thanks the Fulbright Commission for financing his stay at Louisiana State University where part of the research was performed. Access to computing and storage facilities owned by parties and projects contributing to the National Grid Infrastructure MetaCentrum, provided under the program "Projects of Large Infrastructure for Research, Development, and Innovations" (LM2010005), is greatly appreciated.

APPENDIX A: HARTREE-FOCK PHASE BOUNDARY

Initial version of HF equations (10) can be recast into the simpler form (11) by introducing auxiliary quantities $E_d \equiv \Sigma^{\mathrm{HF}} + \varepsilon$ and $\delta \equiv \sum_{\alpha=L,R} \Gamma_\alpha e^{i\Phi_\alpha} - \mathcal{S}^{\mathrm{HF}}$ and further using the general identity

$$-\frac{1}{\beta}\sum_{\omega_n} e^{i\omega_n 0^+} \frac{i\omega_n[1+s(i\omega_n)]}{D(i\omega_n)} = \frac{1}{2} \tag{A1}$$

valid for *any* spin-symmetric GF (4) due to a sum rule reflecting the fundamental anticommutation relation

$$\begin{aligned}\frac{1}{\beta}\sum_{\omega_n} e^{i\omega_n 0^+}[G(i\omega_n)+\bar{G}(i\omega_n)] &= -\frac{1}{\beta}\sum_{\omega_n} e^{i\omega_n 0^+}\frac{2i\omega_n[1+s(i\omega_n)]+\Sigma^*(i\omega_n)-\Sigma(i\omega_n)}{D(i\omega_n)} \\ &= G(\tau-\tau'\to 0^-)+\bar{G}(\tau-\tau'\to 0^-) \equiv \langle d^\dagger d\rangle + \langle d d^\dagger\rangle = 1.\end{aligned} \tag{A2}$$

Large-frequency behavior of the self-energy $\Sigma(i\omega_n)$ is limited by a constant (in case of the HF approximation; otherwise it generically decays as $1/i\omega_n$), which allows us to drop the phase-convergence factor in the above sum, and using the symmetry relations $\Sigma^*(i\omega_n) = \Sigma(-i\omega_n)$ (implying real Σ^{HF}) and $D(-i\omega_n) = D(i\omega_n)$ [Eq. (5)] we get $\sum_{\omega_n} e^{-i\omega_n 0^+}\frac{\Sigma^*(i\omega_n)-\Sigma(i\omega_n)}{D(i\omega_n)} = \sum_{\omega_n}\frac{\Sigma(-i\omega_n)-\Sigma(i\omega_n)}{D(i\omega_n)} = 0$, thus proving the required identity (A1).

Determinant $D^{\mathrm{HF}}(i\omega_n)$ explicitly reads as

$$\begin{aligned}D^{\mathrm{HF}}(i\omega_n) &= \omega_n^2\left[1+\sum_\alpha \frac{\Gamma_\alpha}{\sqrt{\Delta_\alpha^2+\omega_n^2}}\right]^2 + [\varepsilon+\Sigma^{\mathrm{HF}}]^2 + \left|\sum_\alpha \frac{\Gamma_\alpha\Delta_\alpha}{\sqrt{\Delta_\alpha^2+\omega_n^2}}e^{i\Phi_\alpha} - \mathcal{S}^{\mathrm{HF}}\right|^2 \\ &= \omega_n^2\left[1+\sum_\alpha \frac{\Gamma_\alpha}{\sqrt{\Delta_\alpha^2+\omega_n^2}}\right]^2 + E_d^2 + \left|\sum_\alpha \Gamma_\alpha e^{i\Phi_\alpha}\left(\frac{\Delta_\alpha}{\sqrt{\Delta_\alpha^2+\omega_n^2}}-1\right)+\delta\right|^2 \\ &\approx E_d^2 + |\delta|^2 + \left[\left(1+\sum_\alpha\frac{\Gamma_\alpha}{\Delta_\alpha}\right)^2 - \sum_\alpha \frac{\Gamma_\alpha}{\Delta_\alpha^2}\mathrm{Re}(\delta e^{-i\Phi_\alpha})\right]\omega_n^2.\end{aligned} \tag{A3}$$

Because close to the QPT both E_d and δ are close to zero, the second term in the brackets multiplying ω_n^2 can be safely neglected in the calculation of the phase boundary (as is done in the main text) since this term is effectively of higher order in the ω_n expansion.

Finally, we discuss the band contribution term $\mathcal{B}$ [Eq. (14)]. Its name derives from the fact that when the integral over the Matsubara frequencies (14) is Wick rotated to the real frequencies, it only contains the continuous (band) part of the spectrum, i.e., it does not encompass any ABS contributions. The general formula can be recast into a more compact form for the generic case with equal SC gaps $\Delta_L = \Delta_R = \Delta$. Using the substitution $\omega = \Delta\sinh t$ and mutually canceling the common $2\sinh^2\frac{t}{2}$ terms in the numerator and denominator of the integrand, we arrive at the expression

$$\mathcal{B} = \frac{\sum_\alpha \Gamma_\alpha e^{i\Phi_\alpha}}{\Delta}\int_0^{2\pi}\frac{dt}{2\pi}\frac{\cosh^2 t}{\left(\cosh t + \frac{\sum_\alpha\Gamma_\alpha}{\Delta}\right)^2\cosh^2\frac{t}{2} + \left|\frac{\sum_\alpha\Gamma_\alpha e^{i\Phi_\alpha}}{\Delta}\right|^2\sinh^2\frac{t}{2}} \tag{A4}$$

which generalizes the symmetric case $\Gamma_L = \Gamma_R = \Gamma/2$ (and $\Phi_L = -\Phi_R = \Phi/2$) studied previously in Ref. [50].

APPENDIX B: CHARGE CONSERVATION FOR THE DYNAMICAL CORRECTIONS

1. FDC

As a special case of Eq. (7), we now consider the charge conservation in the second-order approximation for which the "current defect" reads as

$$\delta J^{(2)} = -\frac{4}{\beta}\mathrm{Im}\sum_{\omega_n}\mathcal{S}^{(2)}(i\omega_n)\mathcal{G}^*(i\omega_n) \tag{B1}$$

with the anomalous self-energy [Eq. (18b)]

$$\mathcal{S}^{(2)}(i\omega_n) = -\frac{U^2}{\beta}\sum_{\nu_m}\mathcal{G}(i\omega_n + i\nu_m)\chi(i\nu_m), \tag{B2}$$

and the bubble contribution [Eq. (18c)]

$$\chi(i\nu_m) = \frac{1}{\beta}\sum_{\omega_k}[G(i\nu_m + i\omega_k)G(i\omega_k) + \mathcal{G}(i\nu_m + i\omega_k)\mathcal{G}^*(i\omega_k)]. \tag{B3}$$

Separating the quantity $\delta J^{(2)} = \delta J_n^{(2)} + \delta J_a^{(2)}$ into two parts corresponding to the normal and anomalous Green functions constituents of the bubble, respectively, we get

$$\begin{aligned}\delta J_n^{(2)} &= \frac{4U^2}{\beta^3}\mathrm{Im}\sum_{\omega_n,\omega_k,\nu_m} G(i\nu_m + i\omega_k)G(i\omega_k)\mathcal{G}(i\omega_n + i\nu_m)\mathcal{G}^*(i\omega_n),\\ \delta J_a^{(2)} &= \frac{4U^2}{\beta^3}\mathrm{Im}\sum_{\omega_n,\omega_k,\nu_m} \mathcal{G}(i\nu_m + i\omega_k)\mathcal{G}^*(i\omega_k)\mathcal{G}(i\omega_n + i\nu_m)\mathcal{G}^*(i\omega_n).\end{aligned} \tag{B4}$$

Using the symmetry relation $G^*(i\omega) = G(-i\omega)$, we can manipulate the first formula as

$$\begin{aligned}\delta J_n^{(2)} &= \frac{2U^2}{\beta^3}\sum_{\omega_n,\omega_k,\nu_m}[G(i\nu_m + i\omega_k)G(i\omega_k)\mathcal{G}(i\omega_n + i\nu_m)\mathcal{G}^*(i\omega_n) - G^*(i\nu_m + i\omega_k)G^*(i\omega_k)\mathcal{G}^*(i\omega_n + i\nu_m)\mathcal{G}(i\omega_n)]\\ &= \frac{2U^2}{\beta^3}\sum_{\omega_n,\omega_k,\nu_m}[G(i\nu_m + i\omega_k)G(i\omega_k)\mathcal{G}(i\omega_n + i\nu_m)\mathcal{G}^*(i\omega_n) - G(-i\nu_m - i\omega_k)G(-i\omega_k)\mathcal{G}^*(i\omega_n + i\nu_m)\mathcal{G}(i\omega_n)]\\ &= \frac{2U^2}{\beta^3}\sum_{\omega_n,\omega_k,\nu_m}[G(i\nu_m + i\omega_k)G(i\omega_k)\mathcal{G}(i\omega_n + i\nu_m)\mathcal{G}^*(i\omega_n) - G(i\nu_m + i\omega_k)G(i\omega_k)\mathcal{G}^*(i\omega_n - i\nu_m)\mathcal{G}(i\omega_n)]\\ &= 0,\end{aligned} \tag{B5}$$

where we have used substitutions $\omega_k \to -\omega_k$ and $\nu_m \to -\nu_m$ in the second term of the sums between the second and the third lines and then the shift of the summation variable $\omega_n - \nu_m \to \omega_n$ in the last step. Analogously, the anomalous contribution can be simplified with help of the substitution $\nu_m \to -\nu_m$ and shift of variables $\omega_{n,k} \to \omega_{n,k} + \nu_m$ as follows:

$$\begin{aligned}\delta J_a^{(2)} &= \frac{2U^2}{\beta^3}\sum_{\omega_n,\omega_k,\nu_m}[\mathcal{G}(i\nu_m + i\omega_k)\mathcal{G}^*(i\omega_k)\mathcal{G}(i\omega_n + i\nu_m)\mathcal{G}^*(i\omega_n) - \mathcal{G}^*(i\nu_m + i\omega_k)\mathcal{G}(i\omega_k)\mathcal{G}^*(i\omega_n + i\nu_m)\mathcal{G}(i\omega_n)]\\ &= \frac{2U^2}{\beta^3}\sum_{\omega_n,\omega_k,\nu_m}[\mathcal{G}(i\nu_m + i\omega_k)\mathcal{G}^*(i\omega_k)\mathcal{G}(i\omega_n + i\nu_m)\mathcal{G}^*(i\omega_n) - \mathcal{G}^*(-i\nu_m + i\omega_k)\mathcal{G}(i\omega_k)\mathcal{G}^*(i\omega_n - i\nu_m)\mathcal{G}(i\omega_n)]\\ &= 0,\end{aligned} \tag{B6}$$

which finalizes the required proof of the conserving nature $\delta J^{(2)} = 0$ of the FDC approximation.

2. DC

As we have shown numerically in Sec. IV C, the DC approximation is charge conserving for identical gaps $\Delta_L = \Delta_L = \Delta$. This can be proven analytically by showing that both $\mathcal{G}^{\mathrm{DC}}(i\omega_n)$ and $\mathcal{S}^{\mathrm{DC}}(i\omega_n)$ are real, which is a sufficient condition for $\delta J = 0$ in Eq. (B1). By making use of the gauge invariance it is possible to introduce a *global* phase shift

$$\phi_{\mathrm{sh}} = \arctan\left(\frac{\Gamma_L - \Gamma_R}{\Gamma_L + \Gamma_R}\tan\frac{\phi}{2}\right), \tag{B7}$$

such that $\phi_L = \phi_{\mathrm{sh}} - \phi/2$, $\phi_R = \phi_{\mathrm{sh}} + \phi/2$ for which $\Delta_\phi(i\omega_n)$ is real for all frequencies. Consequently, the $\mathcal{G}^{\mathrm{HF}}(i\omega_n)$ and $\mathcal{S}^{\mathrm{HF}}$ are real too because the equality

$$2\,\mathrm{Im}\mathcal{S}^{\mathrm{HF}} = \mathcal{S}^{\mathrm{HF}} - \mathcal{S}^{\mathrm{HF}*} = -2\,\mathrm{Im}\mathcal{S}^{\mathrm{HF}}\frac{U}{\beta}\sum_{\omega_n}\frac{1}{D^{\mathrm{HF}}(i\omega_n)} \tag{B8}$$

can be generally fulfilled only when $\mathrm{Im}\mathcal{S}^{\mathrm{HF}} = 0$. Assuming the contrary, i.e., the existence of the special solution

$$\frac{U}{\beta}\sum_{\omega_n}\frac{1}{D^{\mathrm{HF}}(i\omega_n)} = -1 \tag{B9}$$

implies from Eq. (10) the identity $\frac{U}{\beta}\sum_{\omega_n}\frac{\Delta_\phi(i\omega_n)}{D^{\mathrm{HF}}(i\omega_n)}=0$ which would in turn mean that Eq. (9b) is fulfilled for *any* $\mathcal{S}^{\mathrm{HF}}$. Correspondingly, the same must be true also for Eq. (B9) which can be easily contradicted, e.g., by taking limit $\mathcal{S}^{\mathrm{HF}}\to\infty$. Reality of $\mathcal{G}^{\mathrm{HF}}(i\omega_n)$ then follows directly from Eq. (9c).

The second-order contribution to the anomalous DC self-energy is also real because it reads as

$$\mathcal{S}^{(2)}(i\omega_n)=-\frac{U^2}{\beta}\sum_{\nu_m}\mathcal{G}^{\mathrm{HF}}(i\omega_n+i\nu_m)\chi^{\mathrm{HF}}(i\nu_m), \tag{B10}$$

where both $\mathcal{G}^{\mathrm{HF}}(i\omega_n)$ and the bubble contribution $\chi^{\mathrm{HF}}(i\nu_m)$ [see Eq. (18c)] are real. However, the first-order contribution to the anomalous DC self-energy reads as $\mathcal{S}^{(1)}=\frac{U}{\beta}\sum_{\omega_n}\mathcal{G}^{\mathrm{DC}}(i\omega_n)$ where

$$\mathcal{G}^{\mathrm{DC}}(i\omega_n)=-\frac{1}{D^{\mathrm{DC}}(i\omega_n)}(\mathcal{S}^{(1)}+\mathcal{S}^{(2)}(i\omega_n)-\Delta_\phi(i\omega_n)) \tag{B11}$$

with all $\mathcal{S}^{(2)}(i\omega_n)$, $D^{\mathrm{DC}}(i\omega_n)$, $\Delta_\phi(i\omega_n)$ being real. Therefore, using the same argument as for S^{HF} and $\mathcal{G}^{\mathrm{HF}}(i\omega_n)$, one can show that $\mathcal{S}^{(1)}$ is real. Consequently, also $S^{\mathrm{DC}}=\mathcal{S}^{(1)}+\mathcal{S}^{(2)}$ and $\mathcal{G}^{\mathrm{DC}}(i\omega_n)$ are real, which was to be proven.

Note that this proof does not carry over to the general case $\Delta_L\neq\Delta_R$ due to the lack of existence of a global, i.e., frequency-independent phase shift to make $\Delta_\phi(i\omega_n)$ real for all ω_n's. The DC approximation is thus not conserving for nonidentical leads as revealed in our numerical results, although the observed current conservation breaking is very weak (see Fig. 8).

[1] S. De Franceschi, L. Kouwenhoven, C. Schönenberger, and W. Wernsdorfer, Nat. Nanotechnol. **5**, 703 (2010).

[2] J. A. van Dam, Y. V. Nazarov, E. P. A. M. Bakkers, S. De Franceschi, and L. P. Kouwenhoven, Nature (London) **442**, 667 (2006).

[3] W. Chang, V. E. Manucharyan, T. S. Jespersen, J. Nygård, and C. M. Marcus, Phys. Rev. Lett. **110**, 217005 (2013).

[4] G. Katsaros, P. Spathis, M. Stoffel, F. Fournel, M. Mongillo, V. Bouchiat, F. Lefloch, A. Rastelli, O. Schmidt, and S. De Franceschi, Nat. Nanotechnol. **5**, 458 (2010).

[5] A. Y. Kasumov, R. Deblock, M. Kociak, B. Reulet, H. Bouchiat, I. I. Khodos, Y. B. Gorbatov, V. T. Volkov, C. Journet, and M. Burghard, Science **284**, 1508 (1999).

[6] A. F. Morpurgo, J. Kong, C. M. Marcus, and H. Dai, Science **286**, 263 (1999).

[7] A. Kasumov, M. Kociak, M. Ferrier, R. Deblock, S. Guéron, B. Reulet, I. Khodos, O. Stéphan, and H. Bouchiat, Phys. Rev. B **68**, 214521 (2003).

[8] P. Jarillo-Herrero, J. A. van Dam, and L. P. Kouwenhoven, Nature (London) **439**, 953 (2006).

[9] H. I. Jørgensen, K. Grove-Rasmussen, T. Novotný, K. Flensberg, and P. E. Lindelof, Phys. Rev. Lett. **96**, 207003 (2006).

[10] J. P. Cleuziou, W. Wernsdorfer, V. Bouchiat, T. Ondarcuhu, and M. Monthioux, Nat. Nanotechnol. **1**, 53 (2006).

[11] H. I. Jørgensen, T. Novotný, K. Grove-Rasmussen, K. Flensberg, and P. E. Lindelof, Nano Lett. **7**, 2441 (2007).

[12] K. Grove-Rasmussen, H. I. Jørgensen, and P. E. Lindelof, New J. Phys. **9**, 124 (2007).

[13] E. Pallecchi, M. Gaass, D. A. Ryndyk, and C. Strunk, Appl. Phys. Lett. **93**, 072501 (2008).

[14] Y. Zhang, G. Liu, and C. Lau, Nano Res. **1**, 145 (2008).

[15] H. I. Jørgensen, K. Grove-Rasmussen, K. Flensberg, and P. E. Lindelof, Phys. Rev. B **79**, 155441 (2009).

[16] A. Eichler, R. Deblock, M. Weiss, C. Karrasch, V. Meden, C. Schönenberger, and H. Bouchiat, Phys. Rev. B **79**, 161407 (2009).

[17] G. Liu, Y. Zhang, and C. N. Lau, Phys. Rev. Lett. **102**, 016803 (2009).

[18] J.-D. Pillet, C. H. L. Quay, P. Morfin, C. Bena, A. L. Yeyati, and P. Joyez, Nat. Phys. **6**, 965 (2010).

[19] E. J. H. Lee, X. Jiang, R. Aguado, G. Katsaros, C. M. Lieber, and S. De Franceschi, Phys. Rev. Lett. **109**, 186802 (2012).

[20] R. Maurand, T. Meng, E. Bonet, S. Florens, L. Marty, and W. Wernsdorfer, Phys. Rev. X **2**, 011009 (2012).

[21] J. D. Pillet, P. Joyez, R. Žitko, and M. F. Goffman, Phys. Rev. B **88**, 045101 (2013).

[22] A. Kumar, M. Gaim, D. Steininger, A. Levy Yeyati, A. Martín-Rodero, A. K. Hüttel, and C. Strunk, Phys. Rev. B **89**, 075428 (2014).

[23] R. Delagrange, D. J. Luitz, R. Weil, A. Kasumov, V. Meden, H. Bouchiat, and R. Deblock, Phys. Rev. B **91**, 241401(R) (2015).

[24] C. B. Winkelmann, N. Roch, W. Wernsdorfer, V. Bouchiat, and F. Balestro, Nat. Phys. **5**, 876 (2009).

[25] A. Martín-Rodero and A. Levy Yeyati, Adv. Phys. **60**, 899 (2011).

[26] D. J. Luitz, F. F. Assaad, T. Novotný, C. Karrasch, and V. Meden, Phys. Rev. Lett. **108**, 227001 (2012).

[27] T. Matsuura, Prog. Theor. Phys. **57**, 1823 (1977).

[28] L. I. Glazman and K. A. Matveev, JETP Lett. **49**, 659 (1989).

[29] A. V. Rozhkov and D. P. Arovas, Phys. Rev. Lett. **82**, 2788 (1999).

[30] T. Yoshioka and Y. Ohashi, J. Phys. Soc. Jpn. **69**, 1812 (2000).

[31] F. Siano and R. Egger, Phys. Rev. Lett. **93**, 047002 (2004).

[32] M.-S. Choi, M. Lee, K. Kang, and W. Belzig, Phys. Rev. B **70**, 020502 (2004).

[33] G. Sellier, T. Kopp, J. Kroha, and Y. S. Barash, Phys. Rev. B **72**, 174502 (2005).

[34] T. Novotný, A. Rossini, and K. Flensberg, Phys. Rev. B **72**, 224502 (2005).

[35] C. Karrasch, A. Oguri, and V. Meden, Phys. Rev. B **77**, 024517 (2008).

[36] T. Meng, S. Florens, and P. Simon, Phys. Rev. B **79**, 224521 (2009).
[37] J. Bauer, A. Oguri, and A. C. Hewson, J. Phys.: Condens. Matter **19**, 486211 (2007).
[38] Y. Tanaka, A. Oguri, and A. C. Hewson, New J. Phys. **9**, 115 (2007).
[39] T. Hecht, A. Weichselbaum, J. von Delft, and R. Bulla, J. Phys.: Condens. Matter **20**, 275213 (2008).
[40] A. Oguri, Y. Tanaka, and A. C. Hewson, J. Phys. Soc. Jpn. **73**, 2494 (2004).
[41] A. Martín-Rodero and A. L. Yeyati, J. Phys.: Condens. Matter **24**, 385303 (2012)
[42] A. Oguri, Y. Tanaka, and J. Bauer, Phys. Rev. B **87**, 075432 (2013).
[43] D. J. Luitz and F. F. Assaad, Phys. Rev. B **81**, 024509 (2010).
[44] E. Vecino, A. Martín-Rodero, and A. Levy Yeyati, Phys. Rev. B **68**, 035105 (2003).
[45] A. A. Clerk and V. Ambegaokar, Phys. Rev. B **61**, 9109 (2000).
[46] C. Karrasch, The functional renormalization group for zero-dimensional quantum systems in and out of equilibrium, Ph.D. thesis, RWTH Aachen, 2010.
[47] M. Governale, M. G. Pala, and J. König, Phys. Rev. B **77**, 134513 (2008).
[48] S. Droste, S. Andergassen, and J. Splettstoesser, J. Phys.: Condens. Matter **24**, 415301 (2012).
[49] T. Meng, Andreev bound states in Josephson quantum dot devices, Master's thesis, Institut Néel, CNRS Grenoble, 2009.
[50] M. Žonda, V. Pokorný, V. Janiš, and T. Novotný, Sci. Rep. **5**, 8821 (2015).
[51] V. Janiš, V. Pokorný, and M. Žonda, arXiv:1401.0738v2.
[52] R. Žitko, NRG LJUBLJANA, open source numerical renormalization group code, http://nrgljubljana.ijs.si
[53] R. Žitko and T. Pruschke, Phys. Rev. B **79**, 085106 (2009).
[54] G. Baym and L. P. Kadanoff, Phys. Rev. **124**, 287 (1961).
[55] G. Baym, Phys. Rev. **127**, 1391 (1962).
[56] P. W. Anderson, *Basic Notions Of Condensed Matter Physics* (Westview Press, Boulder, CO, 1997).
[57] V. Janiš and V. Pokorný, Sci. Lett. J. **3**, 66 (2014).
[58] V. Janiš and P. Augustinský, Phys. Rev. B **75**, 165108 (2007).
[59] D. R. Hamann, Phys. Rev. **186**, 549 (1969).
[60] A. Georges, G. Kotliar, W. Krauth, and M. J. Rozenberg, Rev. Mod. Phys. **68**, 13 (1996).
[61] R. Bulla, T. A. Costi, and T. Pruschke, Rev. Mod. Phys. **80**, 395 (2008).
[62] C. Brouder, G. Panati, and G. Stoltz, Phys. Rev. Lett. **103**, 230401 (2009); J. Lischner, J. Deslippe, M. Jain, and S. G. Louie, *ibid.* **109**, 036406 (2012).